PTEP

Prog. Theor. Exp. Phys. **2015**, 033B02 (42 pages)
DOI: 10.1093/ptep/ptv009

Classifying bions in Grassmann sigma models and non-Abelian gauge theories by D-branes

Tatsuhiro Misumi*, Muneto Nitta, and Norisuke Sakai

Department of Physics, and Research and Education Center for Natural Sciences, Keio University, Hiyoshi 4-1-1, Yokohama, Kanagawa 223-8521, Japan
*E-mail: misumi@phys-h.keio.ac.jp, nitta@phys-h.keio.ac.jp, norisuke.sakai@gmail.com

Received September 23, 2014; Revised December 4, 2014; Accepted December 30, 2014; Published March 10, 2015

We classify bions in the Grassmann Gr_{N_F,N_C} sigma model (including the $\mathbb{C}P^{N_F-1}$ model) on $\mathbb{R}^1 \times S^1$ with twisted boundary conditions. We formulate these models as $U(N_C)$ gauge theories with N_F flavors in the fundamental representations. These theories can be promoted to supersymmetric gauge theories and, further, can be embedded into D-brane configurations in type-II superstring theories. We focus on specific configurations composed of multiple fractional instantons, termed neutral bions and charged bions, which are identified as perturbative infrared renormalons by Ünsal and his collaborators [G. V. Dunne and M. Ünsal, J. High Energy Phys. **1211**, 170 (2012); G. V. Dunne and M. Ünsal, Phys. Rev. D **87**, 025015 (2013)]. We show that D-brane configurations, as well as the moduli matrix, offer a very useful tool to classify all possible bion configurations in these models. In contrast to the $\mathbb{C}P^{N_F-1}$ model, there exist Bogomol'nyi–Prasad–Sommerfield (BPS) fractional instantons with topological charges greater than unity (of order N_C) that cannot be reduced to a composite of an instanton and fractional instantons. As a consequence, we find that the Grassmann sigma model admits neutral bions made of BPS and anti-BPS fractional instantons, each of which has a topological charge greater (less) than one (minus one), that are not decomposable into an instanton–anti-instanton pair and the rest. The $\mathbb{C}P^{N_F-1}$ model is found to have no charged bions. In contrast, we find that the Grassmann sigma model admits charged bions, for which we construct exact non-BPS solutions of the field equations.

Subject Index B23, B34, B35, B37

1. Introduction

The extensive studies on QCD with adjoint fermions (adj.) on compactified spacetime have recently revealed the great significance of fractional multi-instanton configurations with zero instanton charge, called "bions" [1–18]. It is known that there exist two types of such bion configurations, including "magnetic (charged) bions" and "neutral bions". While magnetic bions bring about the semiclassical confinement in QCD(adj.) on $\mathbb{R}^3 \times S^1$ [19–29], neutral bions (zero topological charge and zero magnetic charge), which are identified as infrared renormalons in the theory [6–15,30–32], induce a center-stabilizing potential for Wilson line holonomy, and play an essential role in the unambiguous and self-consistent semiclassical definition of quantum field theories through a process known as "resurgence": It has been shown that imaginary ambiguities arising in a neutral bion's amplitude and those arising in non-Borel-summable perturbative series (renormalon ambiguities) cancel each other in the small compactification-scale regime of QCD(adj.) on $\mathbb{R}^3 \times S^1$. This implies that the full semiclassical expansion including perturbative and non-perturbative sectors, "resurgent"

Funded by SCOAP[3]

expansion [33], leads to an unambiguous and self-consistent definition of field theories in the same manner as the Bogomol'nyi–Zinn–Justin (BZJ) prescription in quantum mechanics [34–36].

Bions and the resurgence in low-dimensional models have been extensively investigated for the $\mathbb{C}P^{N-1}$ model [8–10,16,17], principal chiral models [12,15], and quantum mechanics [11,13,14]. In Refs. [8,9], generic arguments on bion configurations were given in the $\mathbb{C}P^{N-1}$ model on $\mathbb{R}^1 \times S^1$ with $\mathbb{Z}_N$ twisted boundary conditions, which is a corresponding situation to the $U(1)^{N-1}$ center-symmetric phase in QCD(adj.), based on the independent instanton description taking account of interactions between far-separated fractional instantons and anti-instantons. According to the study, the imaginary ambiguity in the amplitude of neutral bions has the same magnitude, with an opposite sign, as the leading ambiguity $\left(\sim \mp i\pi e^{-2S_I/N}\right)$ arising from a non-Borel-summable series expanded around a perturbative vacuum. The ambiguities at higher orders are canceled by amplitudes of bion molecules (2-bion, 3-bion, ...), and a full trans-series expansion around the perturbative and non-perturbative vacua results in an unambiguous semiclassical definition of field theories.

Among other things, the 2D $\mathbb{C}P^{N-1}$ model enjoys common features with 4D Yang–Mills theory [37] such as asymptotic freedom, dynamical mass generation, and the presence of instantons [38–41]. Fractional instantons in the $\mathbb{C}P^{N-1}$ model on $\mathbb{R}^1 \times S^1$ with twisted boundary conditions were found in Ref. [42] (see also Refs. [43–46]). Fractional instantons in the Grasssmann sigma model were also found in Refs. [47,48]. Explicit solutions or ansatze corresponding to bion configurations in the $\mathbb{C}P^{N-1}$ model have been investigated recently [10,16,17]. Although fractional instantons are Bogomol'nyi–Prasad–Sommerfield (BPS) solutions [49,50], bions are non-BPS as composites of fractional instantons and anti-instantons. In Ref. [10], such non-BPS solutions were found in the $\mathbb{C}P^{N-1}$ model on $\mathbb{R}^1 \times S^1$ with the $\mathbb{Z}_N$ twisted boundary condition by using the method of Refs. [39–41], which can be saddle points for the trans-series expansion. In our previous work [17] we have studied an ansatz corresponding to neutral bions in the $\mathbb{C}P^{N-1}$ model beyond exact solutions, and have shown that our ansatz is consistent with the result from the far-separated instanton gas calculus [8,9] even from short to large separations.

The purpose of our present work is to classify ansatze corresponding to all possible bion configurations in the $\mathbb{C}P^{N-1}$ and Grassmann sigma models on $\mathbb{R}^1 \times S^1$ with twisted boundary conditions. We study mainly the $\mathbb{Z}_N$ twisted boundary condition for simplicity, although we can easily extend our study to more general twisted boundary conditions. In our study, we introduce a new viewpoint based on D-brane configurations to study bion configurations: The $\mathbb{C}P^{N-1}$ and Grassmann sigma models are formulated as a $U\left(N_C\right)$ gauge theory with N_F flavors in the fundamental representations [51–57], which can be embedded into supersymmetric gauge theories by adding fermions (and scalar fields) appropriately. Sigma model instantons (lumps) in the Grassmann sigma model are promoted to non-Abelian vortices [58–64] (see Refs. [65–69] for a review) in gauge theories, especially those of semi-local type [70,71]. By doing so, the moduli space of BPS vortices (lumps) can be clarified completely in terms of the moduli matrix [66,67]. These theories can be further embedded into Hanany–Witten-type D-brane configurations in type-II string theories [72,73], where vortices can be identified with certain D-branes [58]. The T-duality transformation along S^1 maps vortices to domain walls [74–77], which can be described by kinky D-branes [78,79]. These D-brane configurations were used to study the moduli space of non-Abelian vortices before Refs. [47,48].

In this paper, we show that these D-brane configurations, as well as the moduli matrix, offer very useful tools to classify all possible bion configurations in the Grassmann sigma model including the $\mathbb{C}P^{N-1}$ model, and the corresponding non-Abelian gauge theories. We unexpectedly find that the Grassmann sigma model admits neutral bions made of BPS and anti-BPS fractional instantons, each

of which has a topological charge greater (less) than one (minus one), but it cannot be decomposed into an instanton–anti-instanton pair and the rest. We find that the Grassmann sigma model admits charged bions, while the $\mathbb{C}P^{N-1}$ model does not. There are many different species of fractional instantons in the Grassmann sigma model. Among them, we can choose species of BPS fractional instantons and anti-BPS fractional instantons that are noninteracting and can coexist stably. In such cases, we obtain exact non-BPS solutions representing charged bions. We also calculate the energy density and topological charge density of the bion configurations in these models numerically to obtain their interaction energies, which give valuable information on the interactions between constituent fractional instantons, such as the sign and magnitude of the strength, and the dependence on the separations between constituent fractional instantons.

In Sect. 2, we formulate the Grassmann sigma model $Gr_{N_\mathrm{F},N_\mathrm{C}}$ including the $\mathbb{C}P^{N_\mathrm{F}-1}$ model as $U(N_\mathrm{C})$ gauge theory with N_F Higgs scalar fields in the fundamental representation. We also present BPS equations for BPS vortices or lumps in these theories and the moduli matrix that exhausts the moduli parameters of BPS solutions. In Sect. 3, we introduce D-brane configurations in type-II string theories, which realize our theory on certain D-brane worldvolumes. We then study fractional instantons in Grassmann sigma model $Gr_{N_\mathrm{F},N_\mathrm{C}}$ including the $\mathbb{C}P^{N_\mathrm{F}-1}$ model in terms of D-brane configurations and the moduli matrix. In Sect. 4, we classify neutral bions in the $\mathbb{C}P^{N_\mathrm{F}-1}$ model. In Sect. 5, we classify neutral and charged bions in the Grassmann sigma model $Gr_{N_\mathrm{F},N_\mathrm{C}}$. In Sect. 6, we discuss interaction energy for bions with a change in the distance between fractional instanton constituents. Section 7 is devoted to the summary and discussion. In Appendix A, we discuss solutions of a constraint of the Grassmann sigma model.

2. The $U(N_\mathrm{C})$ gauge theory and Grassmann sigma model

2.1. Gauge theory and moduli matrix

Target spaces of supersymmetric nonlinear sigma models must be Kähler for four supercharges [80] and hyper-Kähler for eight supercharges [81,82]. The $\mathbb{C}P^{N_\mathrm{F}-1}$ and Grassmann sigma models can be obtained from supersymmetric gauge theories with four supercharges [51–53] and eight supercharges [54–57]. In this subsection we consider 2D Euclidean gauge field theories in the flat x^1–x^2 plane with $U(N_\mathrm{C})$ gauge group and N_F flavors of scalar fields in the fundamental representation denoted as an $N_\mathrm{C} \times N_\mathrm{F}$ matrix H. The Lagrangian is given as

$$\mathcal{L}_{\text{gauge}} = \mathrm{Tr}\left[\frac{1}{2g^2}F_{\mu\nu}F_{\mu\nu} + \mathcal{D}_\mu H\left(\mathcal{D}_\mu H\right)^\dagger\right] + \mathrm{Tr}\left[\frac{g^2}{4}\left(v^2\mathbf{1}_{N_\mathrm{C}} - HH^\dagger\right)^2\right], \tag{2.1}$$

where g is the gauge coupling and v is a real positive parameter (the Fayet–Iliopoulos (FI) parameter in the context of supersymmetry) [66,67]. The covariant derivative $\mathcal{D}_\mu$ with the gauge field W_μ and field strength $F_{\mu\nu}$ are defined as $\mathcal{D}_\mu H = (\partial_\mu + iW_\mu)H$, $F_{\mu\nu} = -i[\mathcal{D}_\mu, \mathcal{D}_\nu]$. We use a matrix notation such as $W_\mu = W_\mu^I T_I$, where T_I $(I = 0, 1, 2, \ldots, N_\mathrm{C}^2 - 1)$ are matrix generators of the gauge group G in the fundamental representation satisfying $\mathrm{Tr}(T_I T_J) = \frac{1}{2}\delta_{IJ}$, $[T_I, T_J] = if_{IJ}{}^K T_K$ with T^0 as the $U(1)$ generator. The gauge couplings for $U(1)$ and $SU(N_\mathrm{C})$ are independent, but we have chosen identical values for them to discuss classical field configurations in simple terms.

Since the scalar fields H are massless, the Lagrangian has a global symmetry $SU(N_\mathrm{F})$. It can be embedded into a supersymmetric theory with eight supercharges [66,67]. Consequently, it admits BPS solitons [49,50] that preserve some of the supercharges [83]. The vacuum in this model is characterized by the vanishing vacuum energy

$$HH^\dagger = v^2\mathbf{1}_{N_\mathrm{C}}. \tag{2.2}$$

This condition necessitates some of the scalar fields H being non-vanishing ($\mathrm{rank} H = N_{\rm C}$), implying that the gauge symmetry is completely broken (Higgs phase). This vacuum is called a color–flavor-locked vacuum, where $N_{\rm C}$ out of $N_{\rm F}$ flavors should be chosen to be non-vanishing, leaving only a diagonal $SU(N_{\rm C})$ of color $SU(N_{\rm C})$ and $SU(N_{\rm G})$ subgroup of flavor $SU(N_{\rm F})$ group beside the remaining $SU(N_{\rm F}-N_{\rm C})\times U(1)$ as the global symmetry.

Since we consider two Euclidean dimensions, instantons are the usual vortices with codimension two. The Bogomol'nyi completion [49] can be applied to the Lagrangian $\mathcal{L}$ to give a bound

$$\begin{aligned}\mathcal{L} &= \mathrm{Tr}\left[\frac{1}{g^2}\left(B_3+\frac{g^2}{2}\left(v^2\mathbf{1}_{N_{\rm C}}-HH^\dagger\right)\right)^2+\left(\mathcal{D}_1H+i\mathcal{D}_2H\right)\left(\mathcal{D}_1H+i\mathcal{D}_2H\right)^\dagger\right]\\ &\quad+\mathrm{Tr}\left[-v^2\,B_3+2i\,\partial_{[1}H\mathcal{D}_{2]}H^\dagger\right]\geq \mathrm{Tr}\left[-v^2\,B_3+2i\,\partial_{[1}H\mathcal{D}_{2]}H^\dagger\right]\end{aligned}\tag{2.3}$$

with a magnetic field $B_3\equiv F_{12}$. The bound is saturated if the following BPS vortex equations hold [58,59]:

$$0=\mathcal{D}_1H+i\mathcal{D}_2H,\tag{2.4}$$

$$0=B_3+\frac{g^2}{2}\left(v^2\mathbf{1}_{N_{\rm C}}-HH^\dagger\right).\tag{2.5}$$

When these BPS equations are satisfied, the total energy T is given by

$$T\equiv\int d^2x\mathcal{L}=2\pi v^2\,Q,\tag{2.6}$$

with the topological charge Q (instanton number), defined by

$$Q=-\frac{1}{2\pi}\int d^2x\;\mathrm{Tr}B_3=-\frac{1}{2\pi}\int d^2x\;\mathrm{Tr}\left(\frac{1}{2}\epsilon_{\mu\nu}F_{\mu\nu}\right),\tag{2.7}$$

measuring the winding number of the $U(1)$ part of the broken $U(N_{\rm C})$ gauge symmetry[1].

Let us define $S=S(z,\bar z)\in GL(N_{\rm C},\mathbb{C})$ using a complex coordinate $z\equiv x^1+ix^2$:

$$W_1+iW_2=-i2S^{-1}\bar\partial_zS.\tag{2.8}$$

We can solve [62–64] the first of the BPS equations (2.4) in terms of S,

$$H=S^{-1}H_0(z),\tag{2.9}$$

where $H_0(z)$ is an arbitrary $N_{\rm C}$ by $N_{\rm F}$ matrix whose components are holomorphic with respect to z, which is called the *moduli matrix* of BPS solitons. By defining a gauge-invariant quantity

$$\Omega(z,\bar z)\equiv S(z,\bar z)S^\dagger(z,\bar z),\tag{2.10}$$

the second BPS equations (2.5) can be rewritten as

$$\partial_z\left(\Omega^{-1}\bar\partial_z\Omega\right)=\frac{g^2}{4}\left(v^2\mathbf{1}_{N_{\rm C}}-\Omega^{-1}H_0H_0^\dagger\right).\tag{2.11}$$

We call this the *master equation* for BPS solitons[2]. This equation is expected to give no additional moduli parameters. It was proved for $N_{\rm F}=N_{\rm C}=1$ (the Abrikosov–Nielsen–Olesen (ANO) vortices) [85] and is consistent with the index theorem [58] in general $N_{\rm C}$ and $N_{\rm F}$. Moreover, this fact

[1] Our normalization convention of Q corresponds to that in our previous work [17] divided by 2π, and gives integer values for instantons.

[2] The master equation reduces to the so-called Taubes equation [85] in the case of Abrikosov–Nielsen–Olesen (ANO) vortices ($N_{\rm C}=N_{\rm F}=1$) by rewriting $v^2\Omega(z,\bar z)=|H_0|^2e^{-\xi(z,\bar z)}$ with $H_0=\prod_i(z-z_i)$. Note that $\log\Omega$ is regular everywhere, while ξ is singular at vortex positions. The non-integrability of the master equation has been shown in Ref. [84].

can be easily proved in the strong coupling limit where the gauge theories reduce to the Grassmann sigma model, as we show in the next subsection. Thus we assume that the moduli matrix H_0 describes the moduli space completely.

However, we note that there exists a redundancy in the solution (2.9): the physical quantities H and $W_{1,2}$ are invariant under the following V-transformations:

$$H_0(z) \to H_0'(z) = V(z)H_0(z), \quad S(z,\bar{z}) \to S'(z,\bar{z}) = V(z)S(z,\bar{z}), \tag{2.12}$$

with $V(z) \in GL\left(N_{\rm C},\mathbb{C}\right)$ for $^\forall z \in \mathbb{C}$, whose elements are holomorphic with respect to z. Let us note that Ω is invariant under $U\left(N_{\rm C}\right)$ gauge transformations, but is covariant under the V-transformations:

$$\Omega \to V\Omega V^\dagger. \tag{2.13}$$

Incorporating all possible boundary conditions, we find that the total moduli space of BPS solitons $\mathcal{M}^{\rm total}_{N_{\rm C},N_{\rm F}}$ is given by

$$\mathcal{M}^{\rm total}_{N_{\rm C},N_{\rm F}} = \frac{\left\{H_0(z)|H_0(z) \in M_{N_{\rm C},N_{\rm F}}\right\}}{\left\{V(z)|V(z) \in M_{N_{\rm C},N_{\rm C}}, \det V(z) \neq 0\right\}} \tag{2.14}$$

where $M_{N,N'}$ denotes a set of holomorphic $N \times N'$ matrices [62–64,66,67].

The Lagrangian (2.3) evaluated for the BPS solutions in Eq. (2.9) can be rewritten in terms of the gauge-invariant matrix Ω in Eq. (2.10) as

$$\begin{aligned}\mathcal{L}|_{\rm BPS} &= {\rm Tr}\left[-v^2\, B_3 + 2i\partial_{[1}H\mathcal{D}_{2]}H^\dagger\right]\Big|_{\rm BPS} \\ &= 2v^2\,\bar{\partial}_z\partial_z\left(1 - \frac{4}{g^2c}\bar{\partial}_z\partial_z\right)\log\det\Omega.\end{aligned} \tag{2.15}$$

The last four-derivative term above does not contribute to the total energy if the configuration approaches a vacuum on the boundary. Equation (2.11) implies the asymptotic behavior of the gauge-invariant quantity $\Omega \to \frac{1}{v^2}H_0H_0^\dagger$ at the boundary as $z \to \infty$. Therefore, the topological charge Q and the total energy T of the BPS solitons are given in terms of the moduli matrix H_0 as

$$T|_{\rm BPS} = 2\pi v^2\, Q = -\frac{v^2}{2}i\oint dz\partial_z \log\det\left(H_0H_0^\dagger\right) + {\rm c.c.} \tag{2.16}$$

It is important to recognize that the simple formulas in Eqs. (2.15) and (2.16) are valid only for BPS or anti-BPS solitons. We need to use the original definition of energy density (2.1) to obtain the energy of bions, since bions are non-BPS configurations as composites of BPS and anti-BPS solitons.

2.2. *Grassmann sigma model as a strong coupling limit*

Gauge theories reduce to nonlinear sigma models with target spaces as Grassmann manifolds in the strong gauge coupling limit $g^2 \to \infty$. When they are embedded into supersymmetric gauge theories with four (eight) supercharges, they become (hyper-)Kähler (HK) nonlinear sigma models [80–82] on the Higgs branch [56,86] of gauge theories as their target spaces. This construction of a (hyper-)Kähler manifold is called a (hyper-)Kähler quotient [54,55]. In order to have finite energy

configuration, it is necessary to be at the minimum of the potential, leading to a constraint

$$HH^\dagger = v^2 \mathbf{1}_{N_C}. \tag{2.17}$$

Since the gauge kinetic terms for W_μ disappear in the limit of infinite coupling, gauge fields W_μ become auxiliary fields that can be expressed in terms of scalar fields H through their field equations

$$W_\mu = \frac{i}{2v^2}\left(\partial_\mu H H^\dagger - H\partial_\mu H^\dagger\right) = \frac{i}{v^2}\partial_\mu H H^\dagger. \tag{2.18}$$

After eliminating W_μ, the Lagrangian (2.19) with the constraints (2.2) becomes a nonlinear sigma model,

$$\begin{aligned}\mathcal{L}_{\text{Grassmann}} &= \mathrm{Tr}\left[\left(\partial_\mu + iW_\mu\right)H\left(\left(\partial_\mu + iW_\mu\right)H\right)^\dagger\right] \\ &= \mathrm{Tr}\left[\left(\partial_\mu H - \frac{1}{v^2}\partial_\mu H H^\dagger H\right)\left(\partial_\mu H^\dagger - \frac{1}{v^2}H^\dagger H\partial_\mu H^\dagger\right)\right],\end{aligned} \tag{2.19}$$

with the complex Grassmann manifold Gr_{N_F,N_C} as a target space

$$Gr_{N_F,N_C} \simeq \frac{SU\left(N_F\right)}{SU\left(N_C\right)\times SU\left(N_F - N_C\right)\times U(1)}. \tag{2.20}$$

This is the Grassmann sigma model, which is the main focus of our study. Now one can see that the parameter $1/v$ serves as the coupling constant of the Grassmann sigma model. Let us also note that the $\mathbb{C}P^{N_F-1}$ sigma model is obtained as a special case of the Grassmann sigma model: $Gr_{N_F,N_C=1} = \mathbb{C}P^{N_F-1}$. The topological charge Q in Eq. (2.7) can also be expressed in terms of scalar fields H as

$$Q = \frac{i}{2\pi v^2}\int d^2x \mathrm{Tr}\left(\epsilon_{\mu\nu}\mathcal{D}_\mu H\left(\mathcal{D}_\nu H\right)^\dagger\right) = \frac{i}{2\pi v^2}\int d^2x \epsilon_{\mu\nu}\partial_\mu \mathrm{Tr}\left(H\partial_\nu H^\dagger\right). \tag{2.21}$$

One should note that the procedure leading to the Grassmann sigma model is unrelated to supersymmetry. Therefore, the constraints in Eqs. (2.17) and (2.18) have to be obeyed irrespective of BPS or non-BPS field configurations.

Let us first consider (anti-)BPS solutions. For finite gauge coupling, analytic solutions of BPS equations are not possible. For the Grassmann sigma model corresponding to infinite gauge coupling, one of the BPS equations, the master equation (2.11), becomes identical to the constraint of the Grassmann sigma model in Eq. (2.17) and can be easily solved algebraically:

$$\Omega = v^{-2}H_0 H_0^\dagger. \tag{2.22}$$

As described in Appendix A, we can express the nonnegative Hermitian matrix Ω in terms of a unitary matrix U and a nonnegative diagonal matrix Ω_d as

$$\Omega = U\Omega_d U^\dagger, \quad UU^\dagger = \mathbf{1}_{N_C}. \tag{2.23}$$

We can define the inverse square root $\Omega^{-1/2} = v\left(H_0 H_0^\dagger\right)^{-1/2} = U\Omega_d^{-1/2}U^\dagger$ and use it as a possible $U\left(N_C\right)$ gauge choice of S^{-1} to obtain the physical scalar field H as

$$H = U\Omega_d^{-1/2}U^\dagger H_0, \tag{2.24}$$

which satisfies the constraint of the Grassmann sigma model $HH^\dagger = v^2\mathbf{1}_{N_C}$ in Eq. (2.17), as shown in Appendix A.

Now let us consider general (non-BPS) field configurations of the Grassmann sigma model aiming at bion configurations. Any field configurations H in the Grassmann sigma model should satisfy the

constraint in Eq. (2.17). From experiences in the $\mathbb{C}P^{N_{\rm F}-1}$ model [10,17], we know that bion configurations need not be a solution of field equations. On the other hand, we wish to consider bion field configurations becoming solutions of field equations asymptotically when the constituent fractional instantons are far apart. Therefore, our strategy is the following: we consider non-holomorphic (functions of both $z, \bar{z}$) moduli matrices H_0 corresponding to composites of fractional instantons and anti-instantons, which become non-BPS exact solutions asymptotically as separation goes to infinity. The only additional condition to satisfy is the constraint of the Grassmann sigma model in Eq. (2.17). This is achieved by the formula in Eq. (2.24). It is important to realize that this formula can be regarded merely as a solution of the constraint $HH^\dagger = v^2\mathbf{1}_{N_{\rm C}}$, without any reference to the BPS condition.

To obtain the most general S for any gauge choice of $U\left(N_{\rm C}\right)$ gauge invariance, we have the freedom of using another unitary matrix $\tilde{U} \in U\left(N_{\rm C}\right)$ as

$$S = \tilde{U}\Omega^{1/2}, \quad \tilde{U}\tilde{U}^\dagger = \mathbf{1}_{N_{\rm C}}. \tag{2.25}$$

This unitary matrix $\tilde{U}$ is precisely the freedom of the $U\left(N_{\rm C}\right)$ gauge transformations of the underlying gauge theory.

From the target manifold (2.20), one can easily see that there exists a Seiberg-like duality between theories with the same number of flavors and with two different gauge groups in the case of infinite gauge coupling [56,86]:

$$U\left(N_{\rm C}\right) \leftrightarrow U\left(N_{\rm F} - N_{\rm C}\right). \tag{2.26}$$

This duality is exact in the strong coupling limit of the gauge theory; namely, it holds for the entire Lagrangian of the Grassmann sigma models. One should note that, for each BPS solution of the $U\left(N_{\rm C}\right)$ gauge theory with $N_{\rm F}$ flavors of scalar fields H in the fundamental representations, there exists a corresponding anti-BPS solution of the $U\left(N_{\rm F} - N_{\rm C}\right)$ gauge theory with the same number of flavors of scalar fields $\tilde{H}$ in the fundamental representations and vice versa. Besides the Grassmann sigma model constraint for H,

$$HH^\dagger = v^2\mathbf{1}_{N_{\rm C}}, \tag{2.27}$$

and for $\tilde{H}$ at strong coupling,

$$\tilde{H}\tilde{H}^\dagger = v^2\mathbf{1}_{N_{\rm F}-N_{\rm C}}, \tag{2.28}$$

these solutions must satisfy the following orthogonality constraints:

$$H\tilde{H}^\dagger = 0. \tag{2.29}$$

The boundary conditions for the BPS solution H and the anti-BPS solution $\tilde{H}$ should be chosen to be associated with complementary vacua [74–77,87].

The duality between $U\left(N_{\rm C}\right)$ gauge theories and $U\left(N_{\rm F} - N_{\rm C}\right)$ gauge theories can be formulated in terms of the corresponding moduli matrices H_0 and $\tilde{H}_0$ as

$$H_0\tilde{H}_0^\dagger = 0. \tag{2.30}$$

Together with the complementary boundary conditions, this relation determines $\tilde{H}_0$ uniquely from H_0 up to the V-equivalence (2.12). Although this duality is not exact for finite coupling, there still exists a one-to-one dual map by the relation between the moduli matrix H_0 in the original gauge theory and the $\left(N_{\rm F} - N_{\rm C}\right) \times N_{\rm F}$ moduli matrix $\tilde{H}_0$ of the dual gauge theory.

2.3. $\mathbb{Z}_{N_F}$ twisted boundary conditions and fractional instantons

In this subsection, we introduce a $\mathbb{Z}_{N_F}$ twisted boundary condition in the $U(N_C)$ gauge theory with N_F flavors or the Grassmann sigma model as its strong coupling limit on $\mathbb{R}^1 \times S^1$. The $\mathbb{Z}_{N_F}$ twisted boundary conditions in a compactified direction are expressed in terms of a twisting matrix B as [9,10]

$$H\left(x^1, x^2 + L\right) = B\, H\left(x^1, x^2\right), \quad B = \text{diag.}\left[1, e^{2\pi i/N_F}, e^{4\pi i/N_F}, \ldots, e^{2(N_F-1)\pi i/N_F}\right]. \tag{2.31}$$

The $\mathbb{Z}_{N_F}$ twisted boundary condition breaks the global $SU(N_F)$ symmetry down to $\mathbb{Z}_{N_F}$. Fractional instantons (kink instantons) carry integer multiples of the minimum topological charge $1/N_F$ in the Grassmann sigma models on $\mathbb{R}^1 \times S^1$ with a $\mathbb{Z}_{N_F}$ twisted boundary condition [42,47,48].

When x^2 is compactified with the period L, the lowest mass of the Kaluza–Klein modes is $2\pi/L$. In the case of the $\mathbb{Z}_{N_F}$ twisted boundary condition, the lowest mass is also fractionalized to give $2\pi/(N_F L)$. The fractional instanton is in one-to-one correspondence with the kink [42,47,48] as a function of x^1. The study of BPS equations for kinks in the strong coupling limit reveals that the size of the fractional instanton is given by the inverse of the mass difference associated with the adjacent vacua [66,67,88]. Therefore, the size of an elementary fractional instanton with an instanton charge $1/N_F$ is given by $N_F L/(2\pi)$. When two fractional instantons are compressed together, they can form a compressed fractional instanton, whose size should be half that of the individual fractional instantons. By the same token, n fractional instantons can be compressed together to form compressed n fractional instantons whose size should be $N_F L/(2\pi n)$.

From the next subsection, we make all the dimensionful quantities and parameters dimensionless by using the compact scale L ($L \to 1$), unless we have a special reason to recover the dimension.

3. D-brane configurations for fractional instantons

3.1. D-brane configurations

The gauge theory introduced in the last section can be made $\mathcal{N} = 2$ supersymmetric (with eight supercharges) by doubling the Higgs scalar fields H and adding fermionic superpartners (Higgsino and gaugino) and adjoint scalars (dimensionally reduced gauge fields) [66,67]. Then, the theory can be realized by a D-brane configuration [79]. We first consider the Hanany–Witten brane configuration [72,73]. We are interested in Euclidean space $\mathbb{R} \times S^1$, but we consider a brane configuration in 2+1 dimensions by adding a "time" direction. In Table 1, we summarize the directions in which the D-branes extend. In Fig. 1 the brane configuration is schematically drawn.

The $U(N_C)$ gauge theory is realized on the N_C coincident D3-brane worldvolume, which is stretched between two NS5-branes. The D3-brane worldvolume has a finite length Δx^3 between two NS5-branes, and, therefore, the D3-brane worldvolume theory is $(2+1)$-dimensional $U(N_C)$

Table 1. Brane configuration for k vortices: Branes are extended along directions denoted by ○, and are not extended along directions denoted by −. The symbol × denotes the codimensions of the k D1-branes on the worldvolume of the D3-branes excluding x^3, which is a finite line segment.

	x^0	x^1	x^2	x^3	x^4	x^5	x^6	x^7	x^8	x^9
N_C D3	○	○	○	○	−	−	−	−	−	−
N_F D5	○	○	○	−	○	○	○	−	−	−
2 NS5	○	○	○	−	−	−	−	○	○	○
k D1	○	×	×	−	○	−	−	−	−	−

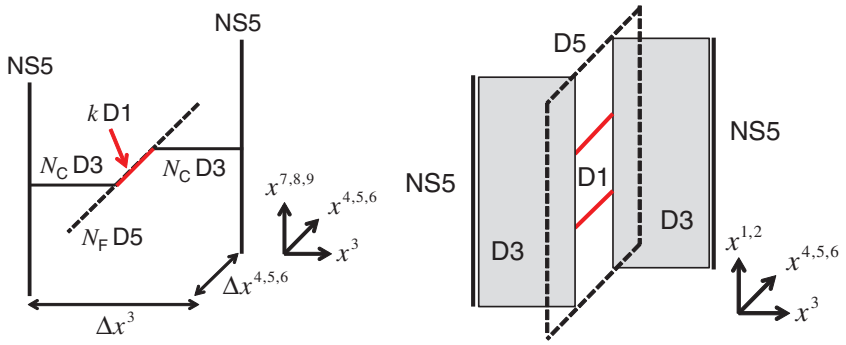

Fig. 1. Brane configuration for k vortices. As for separation of the two NS5-branes, Δx^3 corresponds to $1/g^2$ and $\left(\Delta x^4, \Delta x^5, \Delta x^6\right)$ correspond to the triplet of the FI parameters.

gauge theory with a gauge coupling $\frac{1}{g^2} = |\Delta x^3|\tau_3 l_s^4 = \frac{|\Delta x^3|}{g_s^{(B)}}$, with the string coupling constant $g_s^{(B)}$ in type-IIB string theory and the D3-brane tension $\tau_3 = 1/\left(g_s^{(B)} l_s^4\right)$. The positions of the N_F D5-branes in the x^7-, x^8-, and x^9-directions coincide with those of the D3-branes. Strings that connect between D3- and D5-branes give rise to the N_F hypermultiplets (the Higgs fields H and Higgsinos) in the D3-brane worldvolume theory. The two NS5-branes are separated into the x^4-, x^5-, and x^6-directions, which give the triplet of the FI parameters c^a [58,61]. We choose it as $c^a = \left(0, 0, v^2 = \Delta x^4/\left(g_s^{(B)} l_s^2\right) > 0\right)$, with the string length l_s.

Now, we consider BPS non-Abelian vortices in this setup [58,61]. k vortices are represented by k D1-branes stretched between D3-branes for the following reasons. (1) The D1-branes preserve the half supersymmetry of the D3-brane worldvolume theory. (2) The endpoints of the D1-branes are of codimension two in the D3-brane worldvolume, denoted by the symbol $\times$ in Table 1, since the x^3 direction of the D3-brane worldvolume is finite between the two NS5-branes. (3) The energy $\tau_1 \Delta x^4 = \frac{\Delta x^4}{g_s^{(B)} l_s^2} = v^2$ of each D1-brane coincides with that of a vortex. Therefore, one concludes that the k D1-branes correspond to k vortices in the D3-brane worldvolume theory. When $N_F = N_C$, the vortices are called local vortices, while, for $N_F > N_C$, the vortices are called semi-local vortices.

Next, we compactify the x^2-direction on S^1 with the period L for our purpose. First, we turn on a constant background gauge field

$$A_2 = \text{diag.}\left(m_1, \ldots, m_{N_F}\right) \tag{3.1}$$

on the D5-brane worldvolume as a nontrivial Wilson loop around S^1 on the D5-branes. This precisely gives a twisted boundary condition in our context. In this paper, we consider the $\mathbb{Z}_N$ symmetric twisted boundary condition corresponding to $m_n = 2\pi n/\left(L N_F\right), n = 1, \ldots, N_F$. We then take T-duality along the x^2 direction. Table 2 shows the directions in which the branes extend after T-duality transformation.

With this Wilson loop in Eq. (3.1), the positions of the D4-branes are split into the x^2-direction by an amount

$$X_A = 2\pi l_s^2 m_A \left(A = 1, \ldots, N_F\right). \tag{3.2}$$

These separations give hypermultiplet masses in the D2-brane worldvolume theory. The worldvolume theory of the D2-branes is $(1+1)$-dimensional gauge theory with a gauge coupling $\frac{1}{\hat{g}^2} = \frac{\Delta x^3 l_s}{g_s^{(A)}} = \frac{\Delta x^3 R}{g_s^{(B)}}$ and the FI parameter $\hat{c} = \frac{\Delta x^4}{g_s^{(A)} l_s} = \frac{\Delta x^4 R}{g_s^{(B)} l_s^2}$, where $g_s^{(A)}$ is the string coupling constant in type-IIA string theory.

Table 2. T-dualized configuration: Branes are extended along directions denoted by ○, and are not extended along directions denoted by −. The symbol × denotes the codimensions of the k D2′-branes on the worldvolume of the D2-branes, excluding x^3, which is a finite line segment.

	x^0	x^1	x^2	x^3	x^4	x^5	x^6	x^7	x^8	x^9
N_C D2	○	○	−	○	−	−	−	−	−	−
N_F D4	○	○	−	−	○	○	○	−	−	−
2 NS5	○	○	○	−	−	−	−	○	○	○
k D2′	○	×	○	−	○	−	−	−	−	−
k D2*	○	×	○	○	−	−	−	−	−	−

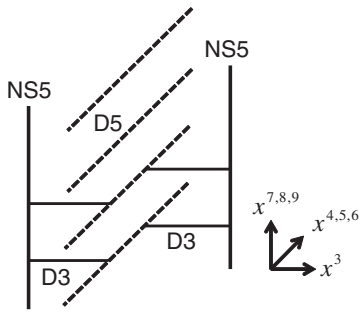

Fig. 2. Vacuum configuration ($k = 0$).

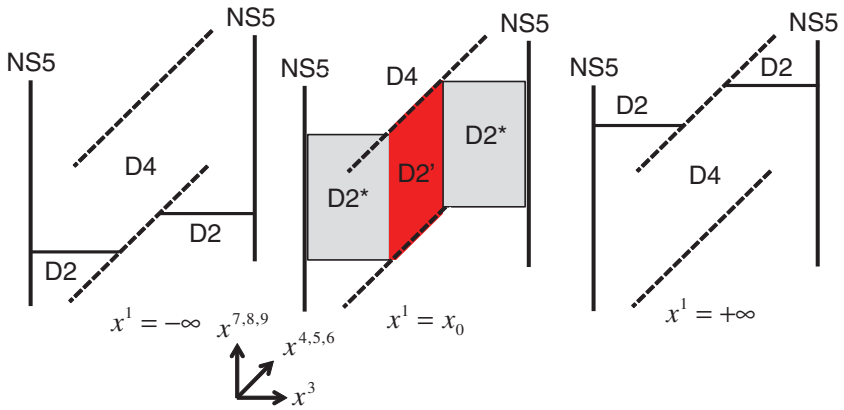

Fig. 3. T-dualized configurations for $k = 1$: the D2′-brane is assumed to be located at $x^1 = x_0$.

First, let us consider vacua without vortices ($k = 0$). As shown in Fig. 2, each D2 -brane ends on one of the D4-branes, on each of which at most one D2-brane can end, which is known as the s-rule [72]. There are ${}_{N_F}C_{N_C} = N_F!/N_C!\big(N_F - N_C\big)!$ vacua in the Grassmann sigma model [57].

Let us consider vortices ($k \neq 0$). The D1-branes representing vortices are mapped by the T-duality to D2-branes, which we denote as D2′, stretched between the D4-branes, as shown in the middle figure in Fig. 3, where the position of the D2′-brane in the x^1 coordinate is denoted as x_0.

The D2-branes are attached to different D4-branes at $x^1 = -\infty$ and $x^1 = +\infty$, and there must exist D2-branes that connect the D2-branes ending on different D4-branes at some point in the x^1-coordinate. These D2-branes correspond to D2′ in Fig. 3. Since the D2′-branes do not end in the x^1-direction, they must be bent to the x^3-direction to end on the NS5-branes. We denote these D2-branes by D2* in Fig. 3. In Fig. 4, the brane configuration in the x^1, x^2, x^3-coordinates is shown. This is nothing but a brane configuration [79] of a BPS kink (domain wall) [74–77] in the

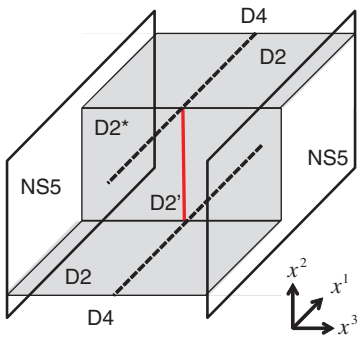

Fig. 4. Brane configuration for a wall.

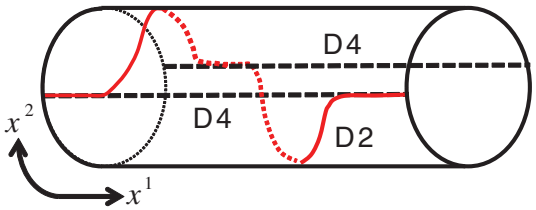

Fig. 5. T-dual picture for $N_{\rm F}=2$, $N_{\rm C}=1$, $k=1$.

D2-brane theory. The energy of the kinks can be calculated from this brane configuration in the strong coupling limit. Since the gauge coupling $\frac{1}{\hat{g}^2}$ is proportional to Δx^3, the D2*-branes disappear in the limit $\hat{g}\to\infty$. The D2′-branes have the energy $\tau_2\,\Delta x^4\,l_s^2\Delta m=\frac{\Delta x^4\Delta m}{g_s^{(A)}l_s}=\hat{c}\,\Delta m$, coinciding with the energy of a kink. A set of D2′+D2*-branes between two D4-branes is a kink as a fractional vortex (or a lump), which corresponds to a fractional instanton in Euclidean $\mathbb{R}\times S^1$ space in our context.

The unit vortex corresponds to the D2-brane winding around the S^1 of the cylinder while exhibiting a kink, as in Fig. 5. The size of the kink in the x^1-direction is that $1/g\sqrt{c}$ of an Abrikosov–Nielsen–Olesen (ANO) vortex. Note that the scalar field $\hat{\Sigma}(x^1)$ has period $1/R$. This vortex can be decomposed into two walls by changing the size of the vortex. In this configuration, the D2-brane is attached to the same D4-brane at $x^1\to\pm\infty$ while exhibiting kinks twice, as in Fig. 5. The relative distance between the two kinks can be interpreted as the size moduli of the single semi-local vortex (or lumps). The small size limit of the configuration reduces to the ANO vortex with the ANO size $1/(gv)$. In other words, the small lump singularity in the strong coupling limit $g\to\infty$ is resolved by the size of the ANO vortex for finite g. By using the brane picture presented here, the moduli space of multiple non-Abelian vortices was classified in Refs. [47,48]. In this paper, we use this kinky D-brane picture to classify all possible bion configurations. We can visualize the kink exhibited in Fig. 5 by using the Wilson loop around the S^1 along x^2 [47,48]:

$$\Sigma(x^1)=-\frac{1}{L}\log\left[\mathbf{P}\exp\int_0^L dx^2 W_2(x^1,x^2)\right], \tag{3.3}$$

where $\mathbf{P}$ is the path-ordering and the gauge field W_2 is given in Eq. (2.18) in the Grassmann sigma model. Since this is a matrix, the intuitive meaning of the brane picture can be best visualized when the matrix $H_0H_0^\dagger$ and Σ are nearly diagonal.

Before doing that, we make a comment on a brane picture of the Seiberg-like duality, which exchanges the gauge group as $U(N_{\rm C})\leftrightarrow U(N_{\rm F}-N_{\rm C})$ in Eq. (2.26). In the Hanany–Witten setup, this is achieved by the exchange of the positions in x^3 of the two NS5-branes. When an NS5-brane

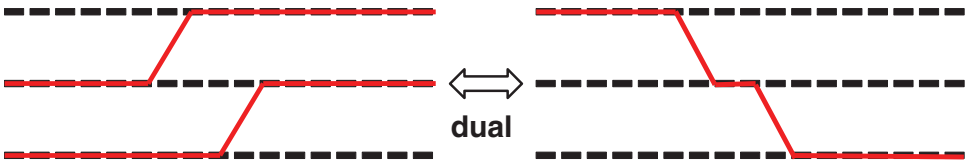

Fig. 6. Brane picture of the Seiberg dual for kinks, where the presence and absence of color branes is exchanged. Here we give an example of the duality between $Gr_{3,2}$ and $Gr_{3,1} \simeq \mathbb{C}P^2$. The horizontal and vertical directions are x^1 and x^2, respectively.

passes through a D5-brane, a D3-brane is created (annihilated) if it is (not) stretched between the NS5-brane and the D5-brane before the crossing, due to the Hanany–Witten effect [72,73]. This changes the number of the D3-branes from $N_{\rm C}$ to $N_{\rm F} - N_{\rm C}$. This exchange flips the sign of the FI parameters $c^a \leftrightarrow -c^a$. The Seiberg dual in the presence of vortices was studied in Ref. [71].

In the T-dual configuration, the presence and absence of D2-branes on D4-branes are exchanged for vacuum configurations. This exchange must hold in the presence of kinky D2-branes since the exchange occurs at every x^1 [79]. This is illustrated in Fig. 6. In this dual transformation, the positions and number of the kinks are unchanged. While the shapes of the kinks would be different for finite gauge couplings, they coincide at strong gauge couplings, where, in the original picture, the positions of the NS5-branes in x^3 coincide with those of the D5-branes.

Now let us summarize how to construct field configurations with the $\mathbb{Z}_{N_{\rm F}}$ twisted boundary condition in the Grassmann sigma model.

1. Because of the color–flavor locking and $\mathbb{Z}_{N_{\rm F}}$ twisted boundary condition, we need to consider a moduli matrix H_0 with each row representing each color line exactly similar to the case of the $\mathbb{C}P^{N_{\rm F}-1}$ model.
2. The V-equivalence allows us to multiply any complex number for each row of H_0. This complex number must be an (anti-)holomorphic function if we wish to construct an (anti-)BPS solution.
3. The (anti-)BPS solution should have H_0 with monotonically increasing (decreasing) color lines.
4. Because of the s-rule [72], no color line occupies the same flavor line in any region of x^1. Consequently, no crossing is allowed for color lines except at isolated points (see reconnection phenomena in later sections).

3.2. *Fractional instantons in the $\mathbb{C}P^{N_{\rm F}-1}$ model $\left(N_{\rm C}=1\right)$*

In terms of the complex coordinate $z = x_1 + ix_2$ on $\mathbb{R}^1 \times S^1$ with $0 \le x_2 < L = 1$, the fractional instantons for the $\mathbb{C}P^1$ model satisfying the $\mathbb{Z}_2$ twisted boundary condition can be parameterized by the following moduli matrices with real moduli parameters $\lambda_L, \lambda_R > 0$ and θ_L, θ_R:

$$H_{0L} = \left(\lambda_L e^{i\theta_L} e^{-\pi z}, 1\right), \quad H_{0R} = \left(\lambda_R e^{i\theta_R} e^{\pi z}, 1\right),$$
$$H_{0L}^* = \left(\lambda_L e^{-i\theta_L} e^{-\pi \bar{z}}, 1\right), \quad H_{0R}^* = \left(\lambda_R e^{-i\theta_R} e^{\pi \bar{z}}, 1\right). \tag{3.4}$$

One should note that the twisted boundary condition automatically introduces nontrivial x^1 dependence in H_0. We call these the elementary fractional instantons.

For sufficiently far left in $x^1 \to -\infty$, H_{0L} (and consequently also the physical field H_L) is dominated by the first component; namely, the configuration is in the first vacuum $H_L \sim \left(ve^{i\theta_1}, 0\right)$. In

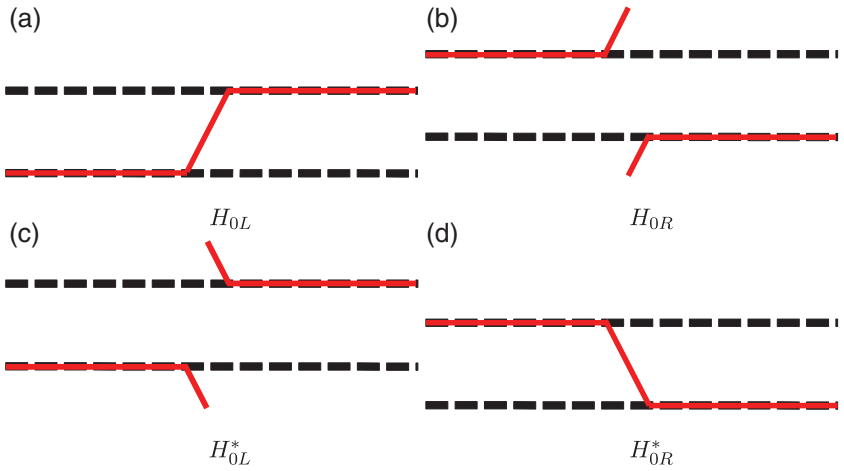

Fig. 7. Brane configurations of fractional instantons in the $\mathbb{C}P^1$ model with the $\mathbb{Z}_2$ twisted boundary condition, corresponding to (a) H_{0L}, (b) H_{0R}, (c) H^*_{0L}, and (d) H^*_{0R}. The horizontal and vertical directions are x^1 and x^2, respectively. The instanton charges Q are (a) $+1/2$, (b) $+1/2$, (c) $-1/2$, (d) $-1/2$, respectively.

contrast, H_{0L} is dominated by the second component at the far right, and H_L is in the second vacuum $H_L \sim \left(0, ve^{i\theta_2}\right)$. The moduli parameter θ_L represents the relative phase $\theta_L = \theta_1 - \theta_2$ between adjacent vacua. In terms of the kinky brane picture, the location of the kink can be defined as the point in x^1 where two components have the same magnitude:

$$\lambda e^{-\pi x^1} = 1 \quad \rightarrow \quad x^1 = \frac{1}{\pi} \log \frac{1}{\lambda}. \tag{3.5}$$

From the T-duality, this is precisely the location of the BPS fractional instanton. Therefore, the fractional (anti-)instanton H_{0L} $\left(H^*_{0L}\right)$ is situated at $x^1 = \frac{1}{\pi} \log \lambda_L$, and the fractional (anti-)instanton H_{0R} $\left(H^*_{0R}\right)$ is at $x^1 = \frac{1}{\pi} \log \frac{1}{\lambda_R}$. Since the moduli matrices H_{0L} and H_{0R} are holomorphic (depend on z only), they give BPS solutions with instanton charge $Q = +1/2$. These two BPS solutions are distinguished only by the label of flavor brane on which the color brane is residing, and are of the same type. On the other hand, H^*_{0L} and H^*_{0R} are anti-holomorphic (depend on $\bar{z}$ only) and give anti-BPS solutions with instanton charge $Q = -1/2$. All of them are (anti-)BPS $\mathbb{C}P^1$ kinks [89–94]. The brane configurations of these solutions are shown in Fig. 7.

In the case of the $\mathbb{C}P^{N_F-1}$ model, we have several kinds of elementary fractional instantons, connecting different adjacent flavors as $\mathbb{C}P^{N-1}$ kinks [95,96]. There can exist elementary and composite fractional instantons. There are N_F different species of elementary fractional instantons: one connecting nth flavor and $(n+1)$th flavor with $1 \leq n \leq N_F$ ($N_F + 1$ identified with 1) is parameterized as

$$\begin{aligned} H_{0n} &= \left(0, \ldots, 0, \lambda_n e^{i\theta_n} e^{-2\pi z/N_F}, 1, 0, \ldots, 0\right), \\ H^*_{0n} &= \left(0, \ldots, 0, \lambda_n e^{-i\theta_n} e^{-2\pi \bar{z}/N_F}, 1, 0, \ldots, 0\right), \end{aligned} \tag{3.6}$$

where the value 1 corresponds to the $(n+1)$th flavor[3]. One should note that the twisted boundary condition automatically introduces nontrivial x^1 dependence in H_0. The BPS solution given by H_{0n}

[3] In the case of $\mathbb{C}P^1$, the moduli matrix H_{0R} is contained in (3.6) as the $n = 2$ case, as one can see by making a V-transformation $\left(\lambda_R e^{i\theta_R} e^{\pi z}, 1\right) \sim \left(1, \lambda_R^{-1} e^{-i\theta_R} e^{-\pi z}\right)$.

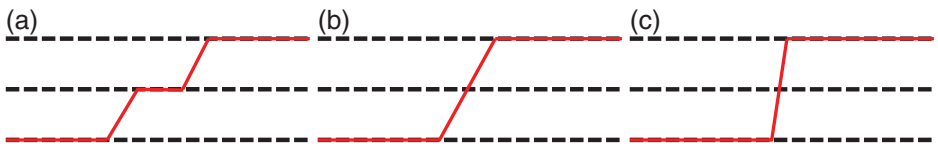

Fig. 8. Composite fractional instantons in the $\mathbb{C}P^2$ model. Keeping the center of mass position $\frac{3}{4\pi}\log\lambda_1$ fixed, (a) generic separated fractional instanton solution $\left(\lambda_1 \approx 1, \lambda_2 \gg 1\right)$, (b) two fractional instantons touching and beginning to merge together $\left(\lambda_1 \approx 1, \lambda_2 \approx 1\right)$, (c) compressed fractional instanton solution $\left(\lambda_1 \approx 1, \lambda_2 \to 0\right)$.

carries an instanton charge $1/N_{\rm F}$, and its conjugate H_{0n}^* carries an instanton charge $-1/N_{\rm F}$. We call these BPS solutions elementary fractional instantons. The fractional instantons for H_{0n} and H_{0n}^* are located at $\frac{N_{\rm F}}{2\pi}\log\lambda_n$. The other moduli θ_n represents the relative phase of the nth and $(n+1)$th vacua. All these elementary fractional instantons are physically distinct, and are needed to form an instanton with unit charge as a composite of fractional instantons, as shown in Fig. 5. In the particular case of the $Z_{N_{\rm F}}$ twisted boundary condition, they are distinct only by the vacuum label n $\left(n = 1, \ldots, N_{\rm F}\right)$ and have identical properties. In that sense, we will exhibit only one of them as representative in the following.

For each topological charge $n/N_{\rm F}$, $n = 1, \ldots, N_{\rm F}-1$, there are $N_{\rm F}$ distinct BPS composite fractional instantons, but we will exhibit only one of them as a kink connecting the first flavor to the $n+1$th flavor, since all other solutions starting from other vacua have identical properties. When the topological charge reaches unity, it becomes a genuine instanton. Those BPS solitons containing at least one instanton are not counted as fractional instantons here. The BPS composite fractional instanton with the maximal topological charge $\left(N_{\rm F}-1\right)/N_{\rm F}$ is given by the moduli matrix

$$H_0 = \left(\lambda_1 e^{i\theta_1} e^{-\frac{(N_{\rm F}-1)}{N_{\rm F}}2\pi z}, \lambda_2 e^{i\theta_2} e^{-\frac{(N_{\rm F}-2)}{N_{\rm F}}2\pi z}, \ldots, \lambda_{N_{\rm F}-1} e^{i\theta_{N_{\rm F}-1}} e^{-\frac{2\pi}{N_{\rm F}}z}, 1\right) \tag{3.7}$$

with $2N_{\rm F}-2$ moduli parameters. Constituent fractional instantons are located at $\frac{N_{\rm F}}{2\pi}\log\frac{\lambda_1}{\lambda_2}$, $\frac{N_{\rm F}}{2\pi}\log\frac{\lambda_2}{\lambda_3}$, $\ldots$, $\frac{N_{\rm F}}{2\pi}\log\frac{\lambda_{N_{\rm F}-2}}{\lambda_{N_{\rm F}-1}}$, $\frac{N_{\rm F}}{2\pi}\log\lambda_{N_{\rm F}-1}$, provided they are ordered as $\frac{N_{\rm F}}{2\pi}\log\frac{\lambda_1}{\lambda_2} < \frac{N_{\rm F}}{2\pi}\log\frac{\lambda_2}{\lambda_3} < \cdots < \frac{N_{\rm F}}{2\pi}\log\frac{\lambda_{N_{\rm F}-2}}{\lambda_{N_{\rm F}-1}} < \frac{N_{\rm F}}{2\pi}\log\lambda_{N_{\rm F}-1}$. If any one of these inequalities is not satisfied, for instance, $\frac{N_{\rm F}}{2\pi}\log\frac{\lambda_n}{\lambda_{n+1}} \geq \frac{N_{\rm F}}{2\pi}\log\frac{\lambda_{n+1}}{\lambda_{n+2}}$, two fractional instantons are merged into one. In the limit of negative infinite relative separation, $\lambda_{n+1} \to 0$, the solution becomes a compressed fractional instanton located at the common center $\frac{N_{\rm F}}{4\pi}\log\frac{\lambda_n}{\lambda_{n+2}}$. In the limit, the size of the compressed fractional instantons becomes half that of the individual fractional instanton.

Figure 8 shows an example in the case of the $\mathbb{C}P^2$ model: two fractional instantons represented by the moduli matrix

$$H_0 = \left(\lambda_1 e^{i\theta_1} e^{-4\pi z/3}, \lambda_2 e^{i\theta_2} e^{-2\pi z/3}, 1\right). \tag{3.8}$$

Fractional instantons are located at $\frac{3}{2\pi}\log\frac{\lambda_1}{\lambda_2}$ and $\frac{3}{2\pi}\log\lambda_2$ in x^1, when $\lambda_2 \gg 1$, as shown in Fig. 8(a). Keeping the center of mass position $\frac{3}{4\pi}\log\lambda_1$ fixed, we can decrease the relative separation $\frac{3}{2\pi}\log\frac{\lambda_1}{\lambda_2^2}$. When $\lambda_2 \approx 1$, two fractional instantons are touching and begin to merge, as shown in Fig. 8(b). When $\lambda_2 \to 0$, the moduli matrix becomes $H_0 = \left(\lambda_1 e^{i\theta_1} e^{-4\pi z/3}, 0, 1\right)$ and two fractional instantons are compressed completely to become a single compressed fractional instanton with a width half that of the individual fractional instanton.

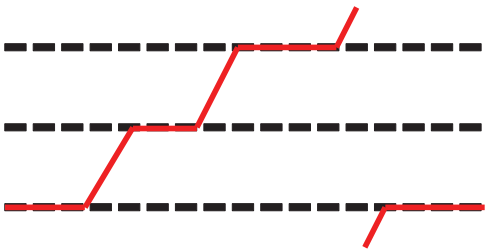

Fig. 9. A $\mathbb{C}P^2$ instanton with the unit instanton charge.

The $\mathbb{C}P^{N_F-1}$ instanton with the unit instanton charge can be obtained with the moduli matrix

$$H_0 = \left(\lambda_1 e^{i\theta_1} e^{-\frac{N_F-1}{N_F}2\pi z} + \lambda_{N_F} e^{i\theta_{N_F}} e^{\frac{2\pi z}{N_F}}, \lambda_2 e^{i\theta_2} e^{-\frac{N_F-2}{N_F}2\pi z}, \ldots, \lambda_{N_F-1} e^{i\theta_{N_F-1}} e^{-\frac{2\pi z}{N_F}}, 1\right). \quad (3.9)$$

Figure 9 shows the BPS instanton in the case of the $\mathbb{C}P^2$ model.

3.3. *Fractional instantons in the Grassmann sigma model*

Now let us move to the Grassmann sigma model, admiting the Grassmann kinks [74–77], which are interpreted as fractional instantons [47,48]. All BPS fractional instanton solutions can be obtained by holomorphic moduli matrices. As described at the end of Sect. 3.1, each of the N_C rows corresponding to each of the N_C color lines of the $U(N_C)$ gauge group can be constructed following precisely the same procedure as in the $N_C = 1$ case $(\mathbb{C}P^{N_F-1}$ model$)$. It is relatively straightforward to construct a moduli matrix H_0 corresponding to the BPS fractional instanton solutions, although computing the inverse square root of the gauge-invariant matrix $(H_0 H_0^\dagger)^{-1/2}$ becomes nontrivial as N_C increases.

For the ath color $(a = 1, \ldots, N_C)$ line in a single row, the increment of the flavor label from the left infinity to the right infinity is denoted as k_a, which corresponds to the numbers of elementary fractional instantons (the instanton charge of k_a/N_F). Then the (anti-)BPS solutions are characterized by a set of nonnegative (nonpositive) integers

$$\left(k_1, k_2, \ldots, k_{N_C}\right), \quad (3.10)$$

corresponding to the number of fractional instantons for each color. This vector of fractional instanton number is used to specify BPS fractional instantons.

To write down the moduli matrix, we need to specify the vacuum on which the soliton is constructed. To classify BPS solutions using the moduli matrix, we introduce a vector of flavor labels f_a occupied by the ath color line in the left vacuum as

$$\left\langle f_1, f_2, \ldots, f_{N_C}\right\rangle. \quad (3.11)$$

This vacuum label for the left vacuum and the vector of fractional instanton number in Eq. (3.10) give a complete characterization of distinct fractional instantons. This characterization is valid even in the case of the non-$\mathbb{Z}_{N_F}$-symmetric boundary condition, unless some of the flavors are degenerated.

Although the flavor label f_1 occupied by the first color is physically distinct from other labels, we only exhibit the case of $f_1 = 1$ here, since cyclic rotations of entire flavor labels give configurations that have the same properties. For instance, we exhibit only one elementary BPS fractional instanton, although there are N_F distinct elementary BPS fractional instantons with identical properties starting

from different vacua. Hence we choose

$$1 = f_1 < f_2 < \cdots < f_{N_C} \leq N_F. \tag{3.12}$$

The s-rule implies that there should be no crossing of color lines and

$$1 + k_1 = f_1 + k_1 < f_2 + k_2 < \cdots < f_{N_C} + k_{N_C} < f_1 + k_1 + N_F. \tag{3.13}$$

To enumerate genuine fractional instantons, we identify a BPS instanton with unit instanton charge as having identical sets of flavors occupied by color lines for left and right vacua

$$1 + k_1 = f_2, \ldots, f_{N_C-1} + k_{N_C-1} = f_{N_C}, \quad f_{N_C} + k_{N_C} = N_F + 1, \tag{3.14}$$

because of $f_1 = 1$.

Similarly to the $\mathbb{C}P^{N_F-1}$ model, many BPS fractional instantons starting from different vacua have identical properties. In the case of the $\mathbb{Z}_{N_F}$ twisted boundary condition, the global $\mathbb{Z}_{N_F}$ symmetry survives. By acting the $\mathbb{Z}_{N_F}$ global transformations, the vacua of the Grassmann sigma model are classified into several equivalence classes. Those BPS solitons starting from the left vacua in the same equivalence class have identical properties, although they are distinct physical solitons. Therefore, we exhibit only the representative for each equivalence class. One should note that all vacua of the $\mathbb{C}P^{N_F-1}$ model $\left(N_C = 1\right)$ are connected by the $\mathbb{Z}_{N_F}$ action and are in one equivalence class.

We need $N_F \geq N_C$ in order to have a ground state with zero energy (supersymmetric vacuum when embedded into a supersymmetric theory). Taking the limit of strong coupling $g^2 \to \infty$ to obtain the Grassmann sigma model requires $N_F > N_C$. Since the $N_C = 1$ case reduces to the previously studied $\mathbb{C}P^{N_F-1}$ models, we consider $N_C \geq 2$. The exact duality between N_C and $N_F - N_C$ in the case of the Grassmann sigma model implies that $Gr_{N_F,N_C=N_F-1} = Gr_{N_F,1} = \mathbb{C}P^{N_F-1}$. Therefore, the simplest Grassmann model beyond $\mathbb{C}P^{N_F-1}$ is the case of $N_C = 2$, $N_F = 4$. The vacua of the Grassmann sigma model $Gr_{4,2}$ falls into two equivalence classes connected by $\mathbb{Z}_{N_F}$ transformations: two colors occupy two adjacent flavors, or two non-adjacent flavors.

Let us exhibit all possible types of BPS and anti-BPS fractional instanton solutions in $Gr_{4,2}$. We first consider the case of left vacua with two adjacent flavors occupied by colors: namely, we consider $f_1 = 1$, $f_2 = 2$. There is only one elementary BPS fractional instanton with total instanton charge $1/4$, specified by $(k_1, k_2) = (0, 1)$, as shown in Fig. 10(a). There are two BPS composite fractional instantons with total instanton charge $1/2$, specified by $(k_1, k_2) = (1, 1)$ and $(0, 2)$, as shown in Fig. 10(b). There is only one BPS composite fractional instanton with total instanton charge $3/4$, specified by $(k_1, k_2) = (1, 2)$, as shown in Fig. 10(c). There are two BPS solutions with total instanton charge 1, specified by $(2, 2)$ and $(1, 3)$. It is surprising and interesting to find that the diagram $(2, 2)$ shown in Fig. 10(e) represents a BPS composite fractional instanton and not an instanton, in spite of the unit total instanton charge. On the other hand, we observe that the $(1, 3)$ diagram is a genuine BPS instanton solution, since the left and right vacua are identical as a set of flavors occupied by colors, as shown in Fig. 10(f). We have listed all BPS solutions with the total instanton charge less than or equal to unity. One can easily check that all other BPS solutions (on this left vacuum with two adjacent flavors occupied by colors) are composites of BPS fractional instantons with at least one genuine BPS instanton.

By the same token, we can list all the anti-BPS solutions as well. The anti-BPS elementary fractional instanton with total instanton charge $-1/4$ is specified by $(-1, 0)$. The composite anti-BPS fractional instantons are $(-2, 0)$ and $(-1, -1)$ with total instanton charge $-1/2$, $(-2, -1)$ with total instanton charge $-3/4$, $(-2, -2)$ with total instanton charge unity. The anti-BPS instanton solution

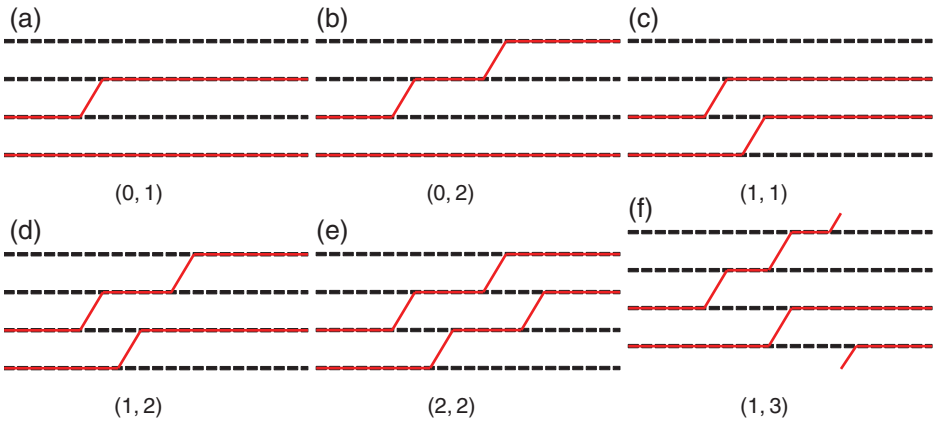

Fig. 10. Fractional instantons for two adjacent flavors occupied by colors at the left vacuum in $Gr_{4,2}$, labeled by indices (a) (0, 1), (b) (0, 2), (c) (1, 1), (d) (1, 2), (e) (2, 2), and (f) (1, 3). Diagram (a) is an elementary fractional instanton, and (b)–(e) are composite fractional instantons. Diagram (f) is an instanton, but not a composite fractional instanton.

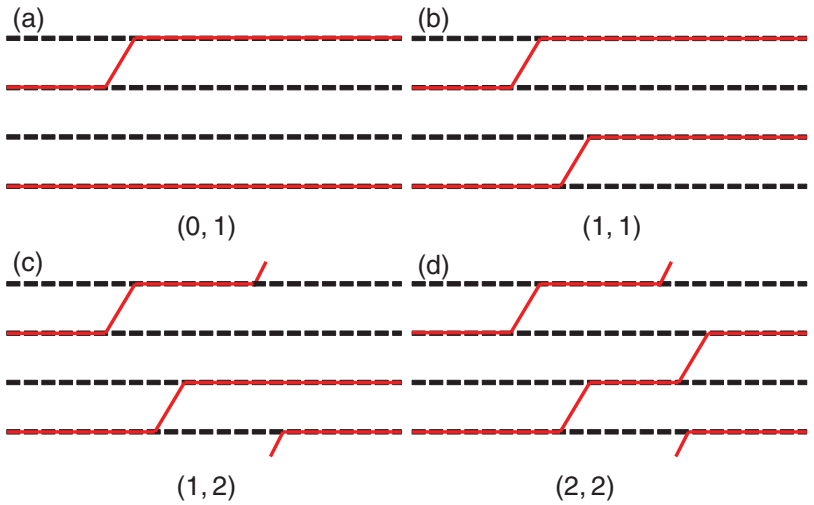

Fig. 11. Fractional instantons for two non-adjacent flavors occupied by colors at the left vacuum in $Gr_{4,2}$, labeled by indices (a) (0, 1), (b) (1, 1), (c) (1, 2), and (d) (2, 2). Diagram (a) is an elementary fractional instanton, (b) and (c) are composite fractional instantons, (d) is a BPS instanton.

is $(-3, -1)$. All other anti-BPS solutions are composites of anti-BPS fractional instantons with at least one genuine anti-BPS instanton.

We can also construct all possible BPS (anti-BPS) solutions for fractional instantons in the other case of left vacua with non-adjacent flavors occupied by colors: namely, we consider $f_1 = 1$, $f_2 = 3$. There is only one type of elementary BPS fractional instanton with total instanton charge $1/4$, specified by $(k_1, k_2) = (0, 1)$, as shown in Fig. 11(a). Let us note that the other possible elementary fractional instanton $(1, 0)$ is of the same type as $(0, 1)$ (although physically distinct) and we do not list it. There is only one type of BPS composite fractional instanton with total instanton charge $1/2$, specified by $(k_1, k_2) = (1, 1)$, as shown in Fig. 11(b). There is only one type of BPS composite fractional instanton with total instanton charge $3/4$, specified by $(k_1, k_2) = (1, 2)$, as shown in Fig. 11(c). $(2, 1)$ is of the same type as $(1, 2)$ and is not listed. There is only one type of BPS solution with total instanton charge 1, specified by $(2, 2)$, as shown in Fig. 11(d). This $(2, 2)$ solution is a genuine BPS

instanton solution, since the left and right vacua are identical as a set of flavors occupied by colors. We have listed all BPS solutions with the total instanton charge less than or equal to unity. One can easily check that all other BPS solutions (on this left vacuum with two non-adjacent flavors occupied by colors) are composites of BPS fractional instantons with at least one genuine BPS instanton.

Summarizing, we find that BPS fractional instantons in the $Gr_{4,2}$ model are exhausted by five species on the left vacuum with two adjacent flavors occupied by colors in Figs. 10(a)–(e), and three species on the left vacuum with two non-adjacent flavors occupied by colors in Figs. 11(a)–(c).

As evidence for the rich varieties of fractional instantons, we observe that BPS fractional instantons not reducible to composites of instantons and fractional instantons can have topological charges of order $N_{\rm C}$ in the case of the $Gr_{N_{\rm F},N_{\rm C}}$ sigma model with large $N_{\rm F}$. By generalizing the (2, 2) fractional instanton for the adjacent vacuum in Fig. 10(e), we obtain a fractional instanton that is characterized by the vector of fractional instanton number $(N_{\rm F}-N_{\rm C},\ldots,N_{\rm F}-N_{\rm C})$ constructed on the vacuum with $N_{\rm C}$ adjacent flavors occupied by colors in the $Gr_{N_{\rm F},N_{\rm C}}$ sigma model. This fractional instanton cannot be reduced to a composite of instanton and fractional instantons by moduli deformations, and has a topological charge $Q=N_{\rm C}\big(N_{\rm F}-N_{\rm C}\big)/N_{\rm F}$, which becomes $Q\sim N_{\rm C}$ for large $N_{\rm F}$.

As an illustrative example, we give explicitly the moduli matrix H_0 for the BPS instanton solution with the set (1, 3) in Fig. 10(f):

$$H_0=\begin{pmatrix}\lambda_1 e^{i\theta_1}e^{-\frac{1}{2}\pi z}, & 1, & 0, & 0\\ 1, & \lambda_3 e^{i\theta_3}e^{-\frac{3}{2}\pi z}, & \lambda_4 e^{i\theta_4}e^{-\pi z}, & \lambda_5 e^{i\theta_5}e^{-\frac{1}{2}\pi z}\end{pmatrix}. \tag{3.15}$$

The constituent fractional instantons are located at $x^1=\frac{2}{\pi}\log\frac{\lambda_3}{\lambda_4}$, $\frac{2}{\pi}\log\frac{\lambda_4}{\lambda_5}$, $\frac{2}{\pi}\log\lambda_1$, $\frac{2}{\pi}\log\lambda_5$. This BPS configuration is nothing but an instanton with the unit instanton charge, as one can recognize from the fact that the set of flavor branes occupied by the color branes in the right infinity of this diagram are identical to the corresponding set at the left infinity. The total instanton charge is of course unity.

As another example, let us write down explicitly the moduli matrix for the BPS solution of (composite) fractional instantons with the set (2, 2), which is depicted in Fig. 10(e):

$$H_0=\begin{pmatrix}\lambda_1 e^{i\theta_1}e^{-\pi z}, & \lambda_2 e^{i\theta_2}e^{-\frac{1}{2}\pi z}, & 1, & 0\\ 0, & \lambda_3 e^{i\theta_3}e^{-\pi z}, & \lambda_4 e^{i\theta_4}e^{-\frac{1}{2}\pi z}, & 1\end{pmatrix}. \tag{3.16}$$

The total instanton number of this BPS solution is unity. However, one should note that the set of flavors occupied by two color branes in the left and right vacua are different. Therefore, this solution is not an instanton, but is a composite soliton of BPS fractional instantons.

In general, fractional instantons are characterized by two adjacent color–flavor-locking vacua, which are denoted by a set of flavors $\big(f_i,\,f_j\big)$ occupied by the first and second colors, respectively, in the case of $N_{\rm C}=2$. The BPS solution defined by the moduli matrix (3.16) is a composite soliton of four different types of fractional instantons. As can be read from the moduli matrix (3.16) for Fig. 10(e), the fractional instanton connecting vacua $(1,2)\to(1,3)$ is located at $\frac{2}{\pi}\log\frac{\lambda_4}{\lambda_5}$, the fractional instanton connecting vacua $(1,3)\to(2,3)$ is located at $\frac{2}{\pi}\log\frac{\lambda_1}{\lambda_2}$, the fractional instanton connecting vacua $(2,3)\to(2,4)$ is located at $\frac{2}{\pi}\log\lambda_5$, and the fractional instanton connecting vacua $(2,4)\to(3,4)$ is located at $\frac{2}{\pi}\log\lambda_2$. In Fig. 10(e), the position of the kink on the first brane at $\frac{2}{\pi}\log\frac{\lambda_1}{\lambda_2}$ is placed to the right of the kink on the second brane at $\frac{2}{\pi}\log\lambda_5$. One should note that their

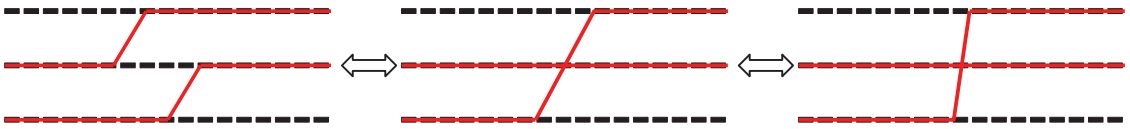

Fig. 12. BPS reconnection. The moduli space of the configuration after BPS reconnection is a boundary of the moduli space of that before BPS reconnection.

positions can be interchanged by taking $\lambda_5 < \frac{\lambda_1}{\lambda_2}$. In that case, the characters of the fractional instantons at these positions change: the fractional instanton connecting vacua $(1,3) \to (1,4)$ is located at $\frac{2}{\pi}\log\lambda_2$, and the fractional instanton connecting vacua $(1,4) \to (2,4)$ is located at $\frac{2}{\pi}\log\frac{\lambda_1}{\lambda_2}$.

Similarly to the $\mathbb{C}P^{N_F-1}$ model, two BPS fractional instantons can be merged together and become a compressed fractional instanton of half the size of the individual fractional instanton in the limit, as illustrated in Fig. 12. This configuration of the compressed fractional instantons can be regarded as a boundary of the moduli space of separated fractional instantons. Since the compressed kink may be regarded as a reconnection of color lines, we call this phenomenon BPS reconnection.

3.4. Energy density of BPS instantons in the Grassmann sigma model

We now calculate the energy density of the BPS instanton configuration in $Gr_{4,2}$ in Fig. 10(f). For this case, the energy density generically depends on x^2, but this dependence disappears as the separation between the fractional instanton constituents gets large. We show here how the lump of the instanton is decomposed into four fractional instantons with the 1/4 topological charge. Figure 13 depicts the energy densities $\mathcal{L}(x^1, x^2)$ in Eq. (2.19) of the instanton in the Grassmann sigma model $Gr_{4,2}$ (Fig. 10(f)) in the x^1 and x^2 plane for three parameter sets. The top one is almost equivalent to the instanton configuration with topological charge being unity, and the x^2 dependence still remains. In the middle one, the instanton starts to be decomposed, and the x^2 dependence is disappearing. In the bottom one, the instanton is almost decomposed into four fractional instantons, and the x^2 dependence disappears.

3.5. Definition of neutral and charged bions

Before ending this section, we give our precise definition of neutral and charged bions in the Grassmann sigma models. It is best described in terms of the vector in Eq. (3.11) to label the left vacua $\langle f_1, \ldots, f_{N_C}\rangle$ and right vacua $\langle f'_1, \ldots, f'_{N_C}\rangle$.

Definition of bions: vanishing total instanton number, namely

$$\sum_{a=1}^{N_C} f_a = \sum_{a=1}^{N_C} f'_a. \tag{3.17}$$

Bions are divided into two types, neutral and charged bions.

1. Neutral bions: the vacuum label vectors in (3.11) in the left and right vacua are identical:

$$f_a = f'_a, \quad a = 1, \ldots, N_C. \tag{3.18}$$

This means that, for both the left and right vacua, the same flavor lines are occupied by color lines.

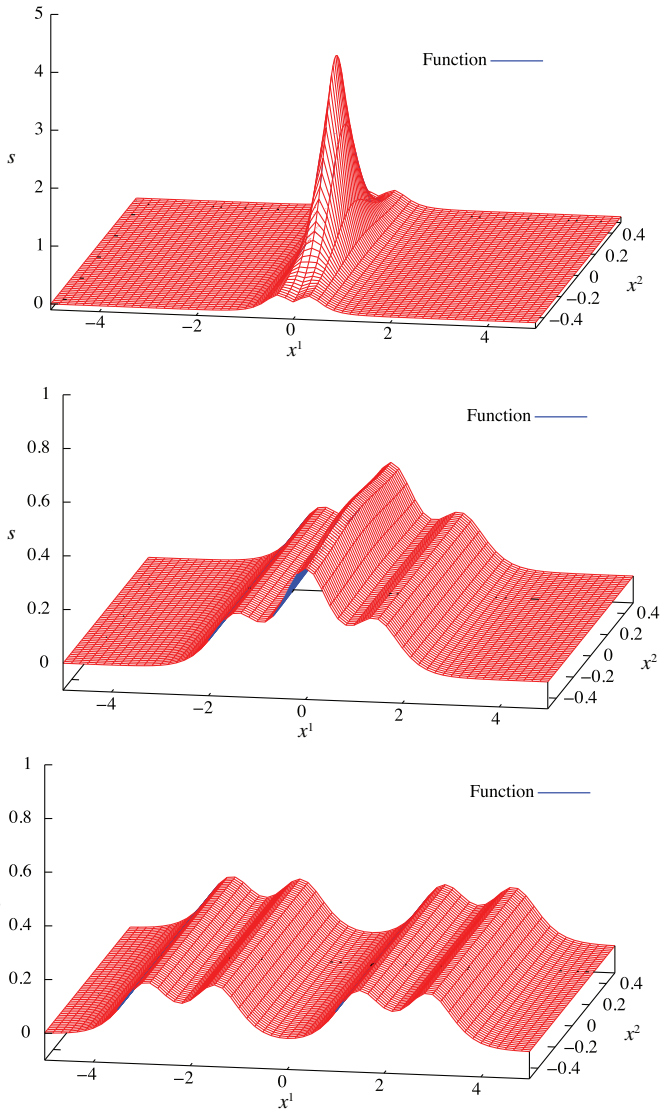

Fig. 13. Energy density $s(\mathbf{x})$ for the BPS instanton configuration of the Grassmann sigma model in Fig. 10(f) for $\lambda_1 = 1,\ \lambda_3 = 1,\ \lambda_4 = 1,\ \lambda_5 = 1$ (top); $\lambda_1 = 1,\ \lambda_3 = 1,\ \lambda_4 = 10,\ \lambda_5 = 10$ (middle); and $\lambda_1 = 10,\ \lambda_3 = 0.1,\ \lambda_4 = 10,\ \lambda_5 = 100$ (bottom). Grassmann sigma model coupling is taken as $v^2 = 1$.

2. Charged bions: the vacuum label vectors in the left and right vacua are different:

$$\langle f_a, f_2, \ldots, f_{N_C} \rangle \neq \langle f'_1, f'_2, \ldots, f'_{N_C} \rangle . \tag{3.19}$$

This means that we have at least one color line that occupies a different flavor line between the left and right vacua.

4. Classification of $\mathbb{C}P^{N_F-1}$ bions

4.1. Bions in the $\mathbb{C}P^1$ model: a review

A neutral bion configuration is a composite of a fractional instanton and fractional anti-instanton with the total instanton charge canceled out. It is a non-BPS configuration and may not be a solution of field equations. Let us discuss the $\mathbb{C}P^1$ model first. From the solutions in Eq. (3.4) and their complex conjugates, it is reasonable to consider the following ansatz for the $\mathbb{C}P^1$ model satisfying

Fig. 14. A neutral bion in the $\mathbb{C}P^1$ model.

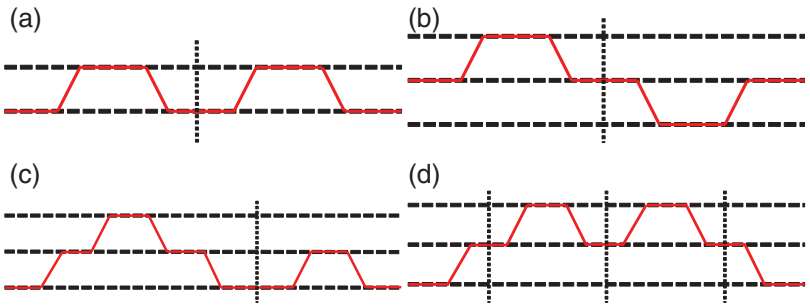

Fig. 15. Reducible neutral bions in the $\mathbb{C}P^{N_F-1}$ model.

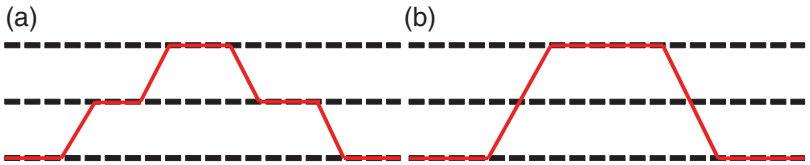

Fig. 16. Irreducible and composite neutral bions in the $\mathbb{C}P^2$ model. (a) Generic position, (b) compressed.

a $\mathbb{Z}_2$ twisted boundary condition (2.31) as [17]:

$$H_0 = \left(\lambda_1 e^{i\theta_1} e^{-\pi z} + \lambda_2 e^{i\theta_2} e^{\pi \bar{z}}, 1\right). \tag{4.1}$$

As shown in Fig. 14, the fractional instanton is located at $\frac{1}{\pi}\log\lambda_1$, and the fractional anti-instanton is at $\frac{1}{\pi}\log\frac{1}{\lambda_2}$. As the separation becomes negative $\lambda_1\lambda_2 \to \infty$ (with λ_1/λ_2 held fixed), they are compressed together and eventually become a vacuum $H_0 \to (1, 0)$.

The energy with arbitrary separation between fractional instanton and anti-instanton was calculated in Ref. [17].

We note that no charged bion is possible in the $\mathbb{C}P^1$ model, which we will explain at the end of the next subsection.

4.2. Bions in the $\mathbb{C}P^{N_F-1}$ model

Let us consider neutral bions in the $\mathbb{C}P^{N_F-1}$ model. A configuration is said to be *reducible* (or *irreducible*) when it can (or cannot) be decomposed into multiple neutral bions by changing the moduli parameters. Examples of reducible and irreducible neutral bions are shown in Figs. 15 and 16, respectively. The configurations in Figs. 15(a)–(c) can be decomposed along the dotted line into two neutral bions, so that they are all reducible. We say that a configuration is reducible even when its subconfiguration can be decomposed into multiple neutral parts. An example of such a configuration is given in Fig. 15(d), where the two regions between the dotted lines are decomposed neutral bions in Fig. 15(a).

Irreducible neutral bions can be characterized in terms of their constituent BPS fractional instanton. We define the topological charge of a neutral bion by the topological charge of the constituent BPS fractional instanton, namely by the number of fractional instantons, which is the same as that of

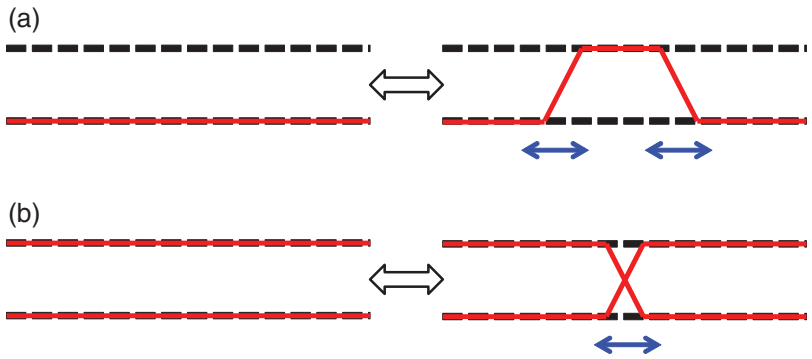

Fig. 17. Fundamental procedures to create neutral bions. (a) Creation of a fractional-instanton–fractional-anti-instanton pair. (b) Crossing/non-BPS reconnection of two color branes. (a) creates neutral bions but (b) does *not*.

fractional anti-instantons because of its neutrality. The total energy is proportional to the topological charge.

For instance, the irreducible bion in Fig. 14 is an elementary-fractional-instanton–elementary-fractional-anti-instanton pair. The simplest example of a neutral bion in the $\mathbb{C}P^2$ model consisting of composite fractional instantons is shown in Fig. 16. This diagram may be regarded as a result of the creation of an elementary-fractional-instanton–anti-instanton pair on the diagram in Fig. 14. One of the characteristic features of composite fractional instantons is that the constituent fractional instantons can merge into a compressed fractional instanton, as shown in Fig. 8. For instance, two fractional (anti-)instantons can merge to form a compressed fractional (anti-)instanton, as shown in Fig. 16.

We note that no charged bion is possible in the $\mathbb{C}P^{N_{\rm F}-1}$ model. This is based on the following reason: For $\mathbb{C}P^{N_{\rm F}-1}$ models, we have only a single color line. Then the zero net instanton charge straightforwardly means that the same flavor line is occupied for the left and right vacua. Our definition of neutral and charged bions in Sect. 3.5 implies that this configuration is nothing but a neutral bion. Thus, all the possible bions (with zero instanton charge) are neutral bions for the $\mathbb{C}P^{N_{\rm F}-1}$ models.

5. Classification of bions in Grassmann sigma models

5.1. Neutral bions in the Grassmann sigma models

In order to classify bions in the Grassmann sigma models systematically, we may consider two fundamental procedures to create neutral bions, as shown in Fig. 17: (a) creation of a fractional-instanton–anti-instanton pair and (b) a crossing of two color branes, which may be called a non-BPS crossing. The pair creation (a) in Fig. 17 increases the number of fractional (anti-)instantons by one, and consequently the topological charge by $1/N_{\rm F}$. The pair creation procedure can be used for constructing neutral bions in the $\mathbb{C}P^{N_{\rm F}-1}$ model. For instance, the neutral bions in Figs. 15 and 16 can be all constructed by repeating the pair creation two and four times, respectively. As we will see later, we can connect the right-hand side of (a) in Fig. 17 with finite energy continuously to the left-hand side of (a) representing the vacuum configuration with vanishing energy by changing the parameters of the field configuration.

On the other hand, we can write down a moduli matrix representing the non-BPS crossing shown in the right-hand side of (b) in Fig. 17 as

$$H_0 = \begin{pmatrix} \lambda_2 e^{i\theta_2} e^{\pi \bar{z}}, & 1 \\ \lambda_1 e^{i\theta_1} e^{-\pi z}, & 1 \end{pmatrix}. \tag{5.1}$$

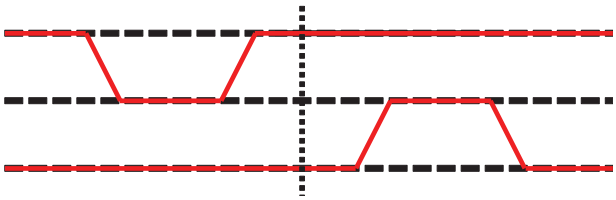

Fig. 18. A reducible neutral bion for the Grassmann sigma models. This is a typical reducible bion in addition to the configurations in Figs. 15(a) and (b), which exist for the $\mathbb{C}P^{N_F-1}$ model. This configuration is a dual to that of Fig. 15(b).

We find the energy density to vanish identically, indicating that the right-hand side of (b) is actually the same as the left-hand side, namely the vacuum itself[4]. Therefore, we do not use the non-BPS crossing in our approach to generate bion configurations in the Grassmann sigma model. It is conceivable that a non-BPS crossing needs to be considered if we consider finite gauge coupling and/or quantum effects properly.

The definition of the reducibility is the same as that in the last subsection for the $\mathbb{C}P^{N_F-1}$ model. In this paper, we classify irreducible neutral bions. In addition to the configurations in Figs. 15(a) and (b), the configuration in Fig. 18 is a reducible neutral bion because each of them can be split into left and right parts. The configuration in Fig. 18 is a Seiberg dual of that of Fig. 15(b). We do not consider these reducible configurations when we classify irreducible neutral bions.

Although we do not consider non-BPS crossing in this work, we here present a case in which the non-BPS crossing and reconnection reduce to the other procedure that we use, namely pair annihilation, as shown in Fig. 19. Instead of considering the reconnection from the non-BPS crossing (b) in Fig. 19 to the vacuum (d) (in the two lower color lines), the non-BPS crossing (b) can be safely deformed by deformations keeping BPS properties to (a) and (c), and then finally (c) to (d) by the pair-annihilation process. Therefore, we find that the non-BPS crossing and reconnection can be reduced to the pair-annihilation process in some region of parameter space by deformations keeping BPS conditions. This result supports our strategy not to use non-BPS crossing to enumerate bion configurations.

When we repeat the insertion of pair creation in Fig. 17(a), we do not insert the second pair outside the first pair, resulting in a zigzag configuration as in Fig. 15(a), which is reducible. Instead, we allow insertion of the second pair creation between the first fractional-instanton–anti-instanton pair, as in Fig. 16(a). If we insert the second pair in an opposite direction to the first one, we again have a zigzag configuration as in Fig. 15(a), which is reducible.

For each color brane, k BPS fractional instantons are placed on the left (right) and k fractional anti-instantons are placed on the right (left) to cancel the instanton charge in total. We label this by k $(-k)$. Therefore, irreducible neutral bions in Gr_{N_F,N_C} can be labeled by a set of N_C integers:

$$(k_1, k_2, \ldots, k_{N_C}), \quad Q = \sum_{a=1}^{N_C} k_a / N_F, \tag{5.2}$$

where $\left(k_1, \ldots, k_{N_C}\right)$ and Q give constituent fractional instanton numbers and the total instanton charge of the BPS fractional instantons corresponding to the left half of the bion.

[4] The matrix is nonsingular $\det H_0 \neq 0$, except possibly at isolated points. Then it is easy to see that H given in our fundamental formula in Eq. (2.24) gives $HH^\dagger = v^2\mathbf{1} = H^\dagger H$. Hence the energy density in Eq. (2.19) vanishes identically.

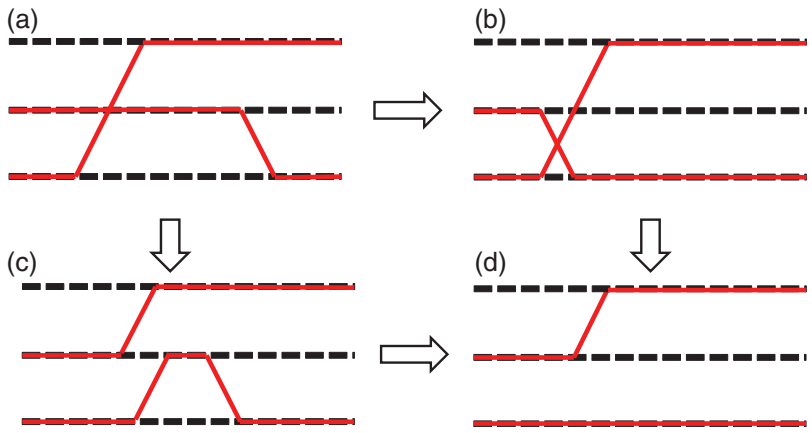

Fig. 19. Annihilation of a compressed kink and a single anti-kink. (a) is the initial configuration of a compressed kink and a single anti-kink, and (d) is the final configuration with one kink. The non-BPS crossing (b) represents a direct collision of an anti-kink with a compressed kink, and can be understood through the BPS reconnection (a) $\to$ (c) to be equivalent to the pair annihilation of a kink and an anti-kink.

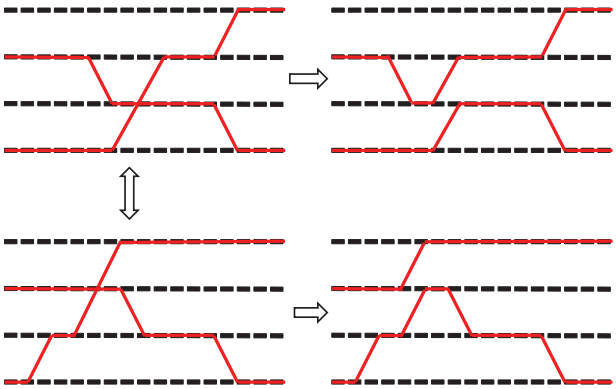

Fig. 20. The upper left and lower left configurations, which are connected to each other by a smooth deformation, become the upper right and lower right configurations, respectively, after BPS reconnections, which are disconnected from each other.

The BPS reconnection in Fig. 12 is always possible, but the configuration after the reconnection is a compressed limit of the configuration before the reconnection. The moduli space of configurations after the BPS reconnection is a boundary of the moduli space of configurations before the BPS reconnection. So we do not regard configurations with one color brane crossing another color brane to be independent. However, note that two moduli that are not connected to each other may be connected by a BPS reconnection, as shown in an example in Fig. 20. A BPS reconnection is always allowed to exhaust all possible configurations, and we have to use it to understand the whole structure of the moduli space.

Now, we are ready to classify all possible irreducible neutral bions in the Grassmann sigma models. As an example, we take the $Gr_{4,2}$ sigma model, which is the simplest Grassmann sigma model. Considering the above arguments, we can obtain all irreducible neutral bions by combining the BPS fractional instantons with the anti-BPS fractional instantons listed in Sect. 3.3.

Let us first consider the case of the left vacuum being two adjacent flavors occupied by color branes. On this vacuum, there are five diagrams of the BPS fractional instantons in Figs. 10(a)–(e). The neutral bions obtained from these fractional instantons are listed in Figs. 21(a)–(e), respectively.

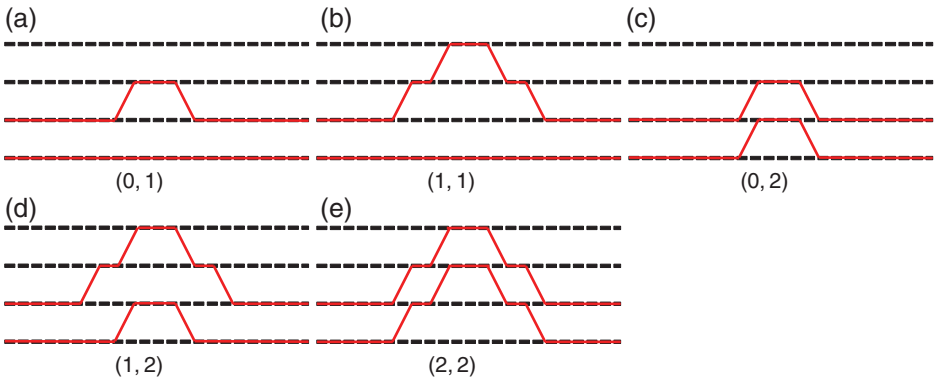

Fig. 21. Neutral bions in $Gr_{4,2}$, labeled by indices (a) (0, 1), (b) (0, 2), (c) (1, 1), (d) (1, 2), (e) (2, 2). (a)–(e) are elementary neutral bions in $Gr_{4,2}$.

We will write down the moduli matrix of these neutral bions explicitly for a more general situation of the $Gr_{N_F,2}$ sigma model. By creating a fractional-instanton–anti-instanton pair on the second color brane in the vacuum, we have Fig. 21(a) with a BPS fractional instanton (0, 1) for the left half of the diagram. The moduli matrix for this (0, 1) neutral bion for the model $Gr_{N_F,2}$ is given by

$$H_0 = \begin{pmatrix} 1, & 0, & 0, & 0, & \dots \\ 0, & \lambda_1 e^{i\theta_1} e^{-\frac{2\pi}{N_F} z} + \lambda_3 e^{i\theta_3} e^{\frac{2\pi}{N_F}\bar{z}}, & 1, & 0, & \dots \end{pmatrix}. \tag{5.3}$$

Similarly to the $\mathbb{C}P^{N_F-1}$ case, the fractional instanton is situated where the magnitudes of two neighboring elements in each row (each color) become equal. In Eq. (5.3), the fractional instanton is located at $x^1 = \frac{N_F}{2\pi}\log\lambda_1$, and the fractional anti-instanton is at $x^1 = \frac{N_F}{2\pi}\log\frac{1}{\lambda_3}$. By creating a fractional-instanton–anti-instanton pair between the fractional-instanton–anti-instanton pair on the second brane in Fig. 21(a), we obtain Fig. 21(b) with a BPS fractional instanton (0, 2) for the left half of the diagram. The moduli matrix for this (0, 2) neutral bion for the model $Gr_{N_F,2}$ is given by

$$H_0 = \begin{pmatrix} 1, & 0, & 0, & 0, & 0, & \dots \\ 0, & \lambda_1 e^{i\theta_1} e^{-\frac{2\pi}{N_F} 2z} + \lambda_5 e^{i\theta_5} e^{\frac{2\pi}{N_F} 2\bar{z}}, & \lambda_2 e^{i\theta_2} e^{-\frac{2\pi}{N_F} z} + \lambda_4 e^{i\theta_4} e^{\frac{2\pi}{N_F}\bar{z}}, & 1, & 0, & \dots \end{pmatrix}. \tag{5.4}$$

The fractional instantons are located at $x^1 = \frac{N_F}{2\pi}\log\lambda_1$, $\frac{N_F}{2\pi}\log\frac{1}{\lambda_2}$, and fractional anti-instantons are at $x^1 = \frac{N_F}{2\pi}\log\frac{1}{\lambda_4}$, $\frac{N_F}{2\pi}\log\frac{\lambda_4}{\lambda_5}$. By creating a fractional-instanton–anti-instanton pair on the first color brane in Fig. 21(a), we obtain Fig. 21(c) with a BPS fractional instanton (1, 1) for the left half of the diagram. The moduli matrix for this (1, 1) neutral bion for the model $Gr_{N_F,2}$ is given by

$$H_0 = \begin{pmatrix} \lambda_1 e^{i\theta_1} e^{-\frac{2\pi}{N_F} z} + \lambda_2 e^{i\theta_2} e^{\frac{2\pi}{N_F}\bar{z}}, & 1, & 0, & 0, & \dots \\ 0, & \lambda_3 e^{i\theta_3} e^{-\frac{2\pi}{N_F} z} + \lambda_4 e^{i\theta_4} e^{\frac{2\pi}{N_F}\bar{z}}, & 1, & 0, & \dots \end{pmatrix}. \tag{5.5}$$

The fractional instantons are located at $x^1 = \frac{N_F}{2\pi}\log\lambda_3$, $\frac{N_F}{2\pi}\log\lambda_1$, and the fractional anti-instantons are at $x^1 = \frac{N_F}{2\pi}\log\frac{1}{\lambda_2}$, $\frac{N_F}{2\pi}\log\frac{1}{\lambda_4}$. To visualize the brane diagram for the bion (1, 1) given by the moduli matrix ansatz (5.5), we computed the relative weight of the absolute value square of each flavor component of the moduli matrix for each row corresponding to the parameter set $\lambda_1 = 10^{-2}$, $\lambda_2 = 10^{-2}$, $\lambda_3 = 10^{-5}$, $\lambda_4 = 10^{-5}$, $N_F = 4$, and plotted them in Fig. 22. Since Σ is almost diagonal when the fractional instantons are far apart, the relative weight becomes indistinguishable from the diagonal elements of Σ given in Eq. (3.3). This result nicely agrees with the schematic picture in Fig. 21(c).

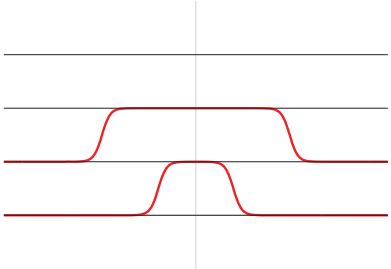

Fig. 22. Brane configuration calculated from the ansatz (5.5) for $\lambda_1 = 10^{-2}, \lambda_2 = 10^{-2}, \lambda_3 = 10^{-5}$, $\lambda_4 = 10^{-5}$, $N_{\rm F} = 4$.

By further creating a fractional-instanton–anti-instanton pair between the fractional-instanton–anti-instanton pair in the second color brane in Fig. 21(c), we obtain Fig. 21(d) with a BPS fractional instanton (1, 2) for the left half of the diagram. The moduli matrix for this (1, 2) neutral bion for the model $Gr_{N_{\rm F},2}$ is given by

$$H_0 = \begin{pmatrix} \lambda_1 e^{i\theta_1} e^{-\frac{2\pi}{N_{\rm F}} z} + \lambda_3 e^{i\theta_3} e^{\frac{2\pi}{N_{\rm F}} \bar{z}}, & 1, & 0, & 0, & 0, & \dots \\ 0, & \lambda_4 e^{i\theta_4} e^{-\frac{2\pi}{N_{\rm F}} 2z} + \lambda_8 e^{i\theta_8} e^{\frac{2\pi}{N_{\rm F}} 2\bar{z}}, & \lambda_5 e^{i\theta_5} e^{-\frac{2\pi}{N_{\rm F}} z} + \lambda_7 e^{i\theta_7} e^{\frac{2\pi}{N_{\rm F}} \bar{z}}, & 1, & 0, & \dots \end{pmatrix}. \tag{5.6}$$

The fractional instantons are located at $x^1 = \frac{N_{\rm F}}{2\pi} \log \frac{\lambda_4}{\lambda_5}, \frac{N_{\rm F}}{2\pi} \log \lambda_5, \frac{N_{\rm F}}{2\pi} \log \lambda_1$, and the fractional anti-instantons are at $x^1 = \frac{N_{\rm F}}{2\pi} \log \frac{1}{\lambda_3}, \frac{N_{\rm F}}{2\pi} \log \frac{1}{\lambda_7}, \frac{N_{\rm F}}{2\pi} \log \frac{\lambda_7}{\lambda_8}$. If we further create a fractional-instanton–anti-instanton pair between the innermost fractional-instanton–anti-instanton pair in the first color brane in Fig. 21(d), we obtain Fig. 21(e) with a BPS fractional instanton (2, 2) for the left half of the diagram. The moduli matrix for this (2, 2) neutral bion for the model $Gr_{N_{\rm F},2}$ is given by

$$H_0 = \begin{pmatrix} \lambda_1 e^{i\theta_1} e^{-\frac{2\pi}{N_{\rm F}} 2z} + \lambda_5 e^{i\theta_5} e^{\frac{2\pi}{N_{\rm F}} 2\bar{z}}, & 0 \\ \lambda_2 e^{i\theta_2} e^{-\frac{2\pi}{N_{\rm F}} z} + \lambda_4 e^{i\theta_4} e^{\frac{2\pi}{N_{\rm F}} \bar{z}}, & \lambda_6 e^{i\theta_6} e^{-\frac{2\pi}{N_{\rm F}} 2z} + \lambda_{10} e^{i\theta_{10}} e^{\frac{2\pi}{N_{\rm F}} 2\bar{z}} \\ 1, & \lambda_7 e^{i\theta_7} e^{-\frac{2\pi}{N_{\rm F}} z} + \lambda_9 e^{i\theta_9} e^{\frac{2\pi}{N_{\rm F}} \bar{z}} \\ 0 & 1 \\ 0, & 0 \\ \vdots & \vdots \end{pmatrix}^T. \tag{5.7}$$

The fractional instantons are located at $x^1 = \frac{N_{\rm F}}{2\pi} \log \frac{\lambda_6}{\lambda_7}, \frac{N_{\rm F}}{2\pi} \log \frac{\lambda_1}{\lambda_2}, \frac{N_{\rm F}}{2\pi} \log \lambda_7, \frac{N_{\rm F}}{2\pi} \log \lambda_2$, and the fractional anti-instantons are at $x^1 = \frac{N_{\rm F}}{2\pi} \log \frac{1}{\lambda_4}, \frac{N_{\rm F}}{2\pi} \log \frac{1}{\lambda_9}, \frac{N_{\rm F}}{2\pi} \log \frac{\lambda_4}{\lambda_5}, \frac{N_{\rm F}}{2\pi} \log \frac{\lambda_9}{\lambda_{10}}$.

There are other diagrams as a composite of BPS solutions and anti-BPS solutions with the set of higher fractional instanton numbers (k_1, k_2), but they contain at least one instanton and are not bions anymore, or reducible diagrams. For instance, if we create a fractional-instanton–anti-instanton pair between the innermost fractional-instanton–anti-instanton pair in the second color brane of (1, 2) in Fig. 21(d), we obtain Fig. 23(a) with a BPS configuration (1, 3) for the left half of the diagram. Since this left half of the brane diagram is the BPS instanton (1, 3) in Fig. 10(f), Fig. 23(a) represents an instanton–anti-instanton pair with the unit instanton charges. The moduli matrix for this (1, 3)

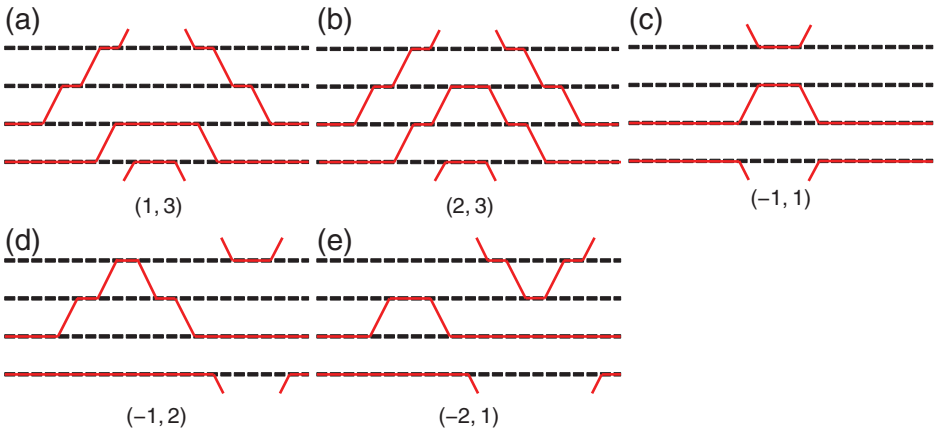

Fig. 23. Solitons in $Gr_{4,2}$ labeled by (a) $(1,3)$, (b) $(2,3)$, (c) $(-1,1)$, (d) $(-1,2)$, and (e) $(-2,1)$, are not elementary neutral bions in $Gr_{4,2}$. (a) $(1,3)$ is an instanton–anti-instanton pair and is not a bion. (b) $(2,3)$ is not an elementary bion anymore because of the decomposition $(2,3)=(1,3)+(1,0)$, where the former is an instanton–anti-instanton pair. (c) is composite. (d) and (e) are not elementary neutral bions that can be understood in dual pictures.

instanton–anti-instanton pair for the model $Gr_{N_{\rm F},2}$ is given by

$$H_0=\begin{pmatrix} \lambda_1 e^{i\theta_1}e^{-\frac{2\pi}{N_{\rm F}}z}+\lambda_3 e^{i\theta_3}e^{\frac{2\pi}{N_{\rm F}}\bar{z}}, & 0 \\ 1, & \lambda_4 e^{i\theta_4}e^{-\frac{2\pi}{N_{\rm F}}3z}+\lambda_{10}e^{i\theta_{10}}e^{\frac{2\pi}{N_{\rm F}}3\bar{z}} \\ 0, & \lambda_5 e^{i\theta_5}e^{-\frac{2\pi}{N_{\rm F}}2z}+\lambda_9 e^{i\theta_9}e^{\frac{2\pi}{N_{\rm F}}2\bar{z}} \\ 0, & \lambda_6 e^{i\theta_6}e^{-\frac{2\pi}{N_{\rm F}}z}+\lambda_8 e^{i\theta_8}e^{\frac{2\pi}{N_{\rm F}}\bar{z}} \\ 0, & 1 \\ 0, & 0 \\ \vdots & \vdots \end{pmatrix}^T. \tag{5.8}$$

The fractional instantons are located at $x^1=\frac{N_{\rm F}}{2\pi}\log\frac{\lambda_6}{\lambda_7}$, $\frac{N_{\rm F}}{2\pi}\log\frac{\lambda_1}{\lambda_2}$, $\frac{N_{\rm F}}{2\pi}\log\lambda_7$, $\frac{N_{\rm F}}{2\pi}\log\lambda_2$, and the fractional anti-instantons are at $x^1=\frac{N_{\rm F}}{2\pi}\log\frac{1}{\lambda_4}$, $\frac{N_{\rm F}}{2\pi}\log\frac{1}{\lambda_9}$, $\frac{N_{\rm F}}{2\pi}\log\frac{\lambda_4}{\lambda_5}$, $\frac{N_{\rm F}}{2\pi}\log\frac{\lambda_9}{\lambda_{10}}$.

The brane diagram in Fig. 23(b) is characterized by $(2,3)$, and is a reducible neutral bion diagram because of the decomposition $(2,3)=(1,3)+(1,0)$; namely, it is a composite of an instanton–anti-instanton pair $(1,3)$ and a fractional instanton $(1,0)$. Figure 23(c) is characterized by $(-1,1)$, and is constructed by placing in the left half of the diagram the exact non-BPS charged bion solution in Fig. 21(g). This is a reducible neutral bion diagram. In general, all the exact non-BPS solutions that we can construct in the moduli matrix formalism are examples of composites of noninteracting BPS and anti-BPS fractional instantons. Therefore, neutral bions constructible from these non-BPS exact solutions are always reducible. The brane diagrams in Figs. 23(d) and (e) are characterized by $(-1,2)$ and $(-2,1)$, respectively. They are reducible neutral bion diagrams because they contain a configuration in Fig. 18.

Lastly, let us consider the other case of the left vacuum being two non-adjacent flavor branes occupied by color branes. We can obtain neutral bions by combining BPS fractional instantons in Figs. 11(a)–(d) with corresponding anti-BPS fractional instantons. The elementary neutral bion in

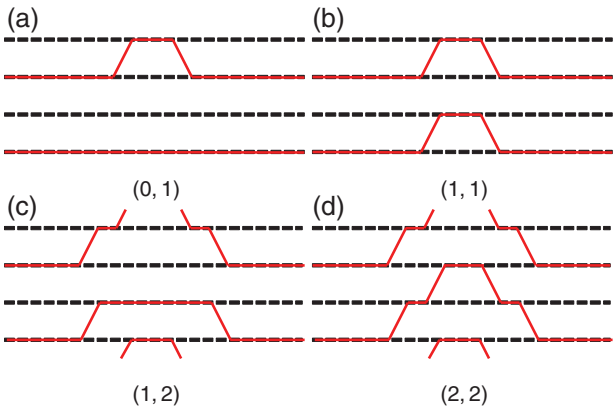

Fig. 24. Neutral bions in $Gr_{4,2}$ for the left vacuum with non-adjacent flavors occupied by colors, labeled by indices (a) (0, 1), (b) (1, 1), (c) (1, 2), and (d) (2, 2). (a) (0, 1) is an elementary neutral bion in $Gr_{4,2}$. (b) (1, 1) is a reducible diagram. (c) (1, 2) is a neutral bion. (d) (2, 2) is a composite of an instanton–anti-instanton pair and is not a neutral bion anymore.

Fig. 24(a) with an elementary BPS fractional instanton (0, 1) for the left half of the diagram is given by the moduli matrix

$$H_0 = \begin{pmatrix} 1, & 0, & 0, & 0, & 0 & \dots \\ 0, & 0, & \lambda_1 e^{i\theta_1} e^{-\frac{2\pi}{N_F} z} + \lambda_3 e^{i\theta_3} e^{\frac{2\pi}{N_F} \bar{z}}, & 1, & 0, & \dots \end{pmatrix}. \tag{5.9}$$

The fractional instanton is located at $x^1 = \frac{N_F}{2\pi} \log \lambda_1$, and the fractional anti-instanton is at $x^1 = \frac{N_F}{2\pi} \log \frac{1}{\lambda_3}$. Two color lines of (1, 1) in Fig. 24(b) do not share any common flavor lines. This is the case of a composite of two noninteracting elementary fractional instantons whose moduli matrix can be given as

$$H_0 = \begin{pmatrix} \lambda_3 e^{i\theta_3} e^{-\frac{2\pi}{N_F} z} + \lambda_4 e^{i\theta_4} e^{\frac{2\pi}{N_F} \bar{z}}, & 1, & 0, & 0, & 0 & \dots \\ 0, & 0, & \lambda_1 e^{i\theta_1} e^{-\frac{2\pi}{N_F} z} + \lambda_2 e^{i\theta_2} e^{\frac{2\pi}{N_F} \bar{z}}, & 1, & 0, & \dots \end{pmatrix}. \tag{5.10}$$

The neutral bion in Fig. 24(c) with a BPS fractional instanton (1, 2) for the left half of the diagram is given by the moduli matrix

$$H_0 = \begin{pmatrix} \lambda_1 e^{i\theta_1} e^{-\frac{2\pi}{N_F} z} + \lambda_3 e^{i\theta_3} e^{\frac{2\pi}{N_F} \bar{z}}, & 0 \\ 1, & 0 \\ 0 & \lambda_4 e^{i\theta_4} e^{-\frac{2\pi}{N_F} 2z} + \lambda_8 e^{i\theta_8} e^{\frac{2\pi}{N_F} 2\bar{z}} \\ 0, & \lambda_5 e^{i\theta_5} e^{-\frac{2\pi}{N_F} z} + \lambda_7 e^{i\theta_7} e^{\frac{2\pi}{N_F} \bar{z}} \\ 0, & 1 \\ 0, & 0, \\ \vdots & \vdots \end{pmatrix}^T. \tag{5.11}$$

The fractional instantons are located at $x^1 = \frac{N_F}{2\pi} \log \frac{\lambda_4}{\lambda_5}$, $\frac{N_F}{2\pi} \log \lambda_5$, $\frac{N_F}{2\pi} \log \lambda_1$, and the fractional anti-instantons are at $x^1 = \frac{N_F}{2\pi} \log \frac{1}{\lambda_3}$, $\frac{N_F}{2\pi} \log \frac{1}{\lambda_7}$, $\frac{N_F}{2\pi} \log \frac{\lambda_7}{\lambda_8}$. One can think of another possibility for (2, 1), but this case is equivalent to the (1, 2) case and is not listed here.

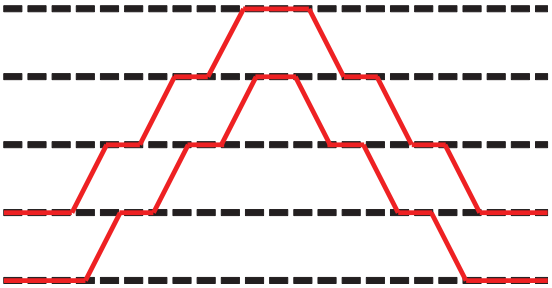

Fig. 25. An irreducible neutral bion with an instanton charge larger than one in $Gr_{5,2}$.

Summarizing, all possible types of irreducible neutral bion configurations for $Gr_{4,2}$ are exhaustively listed as eight possibilities in Figs. 21(a)–(e) and 24(a)–(c). With the same procedures, we can exhaust all possible irreducible neutral bions in the general Gr_{N_F,N_C} model.

In this smallest Grassmann sigma model $Gr_{4,2}$, we encountered a neutral bion whose constituent fractional instanton has unit instanton charge but is different from a genuine instanton, as shown in Fig. 21(e). For larger Grassmann sigma models, there exist neutral bions with instanton charges even larger than one. In Fig. 25, we show a neutral bion in $Gr_{5,2}$, half of which has an instanton charge $6/5$ greater than one. This cannot be decomposed into an instanton and the rest. This kind of phenomenon arises due to an increasingly large number of different species of fractional instantons as N_F, N_C increases.

5.2. Charged bions in the Grassmann sigma models

Charged bions have no instanton charge in total but a nonzero vector of fractional instanton numbers for the whole field configuration. Although the $\mathbb{C}P^{N_F-1}$ models do not admit charged bions, the Grassmann sigma models do.

For a given charged bion configuration, it is always possible to insert neutral bions. Namely, as classification of charged bions, we remove all neutral bions to obtain "purely charged bions." Insertion of neutral bions in general gives physically distinct contributions, but we can choose the representative of cohomology classes as purely charged bions. Thus we obtain a constraint for purely charged bions that each color brane must be either BPS or anti-BPS. This drastically simplifies the classification. We label purely charged bions by a vector of the number of fractional instantons n_a for the ath color brane

$$[n_1, n_2, \ldots, n_{N_C}] \tag{5.12}$$

with the constraint

$$0 = \sum_{a=1}^{N_C} n_a, \tag{5.13}$$

where we use the notation [ ] to distinguish it from the vector ( ) specifing the BPS fractional instantons and neutral bions made from them.

For $Gr_{4,2}$, there is only one possible charged bion $[1, -1]$ on the left vacuum with adjacent flavors occupied by colors, shown in Fig. 26(a). If one wants to increase the vector of fractional instanton numbers to $[2, -2]$, a non-BPS crossing is inevitable, and no new charged bion can be generated. No charged bion is possible for the left vacuum with non-adjacent flavors occupied by colors.

We note that the BPS (monotonically increasing) and anti-BPS (monotonically decreasing) color lines in this charged bion share no flavors in common. This feature is generic for charged bions, since

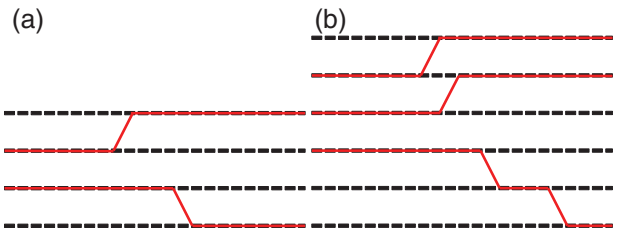

Fig. 26. Non-BPS exact solutions of charged bions in the Grassmann sigma models. (a) Only one possible charged bion in $Gr_{4,2}$. (b) An example of a charged bion in $Gr_{6,3}$.

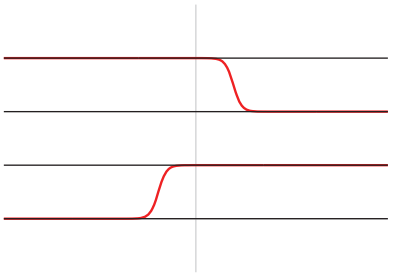

Fig. 27. The brane configuration calculated from the ansatz (5.14) of the exact non-BPS solution of the charged bion for $\lambda_1 = 10^2$, $\lambda_2 = 10^2$, $N_{\rm F} = 4$.

we do not allow color lines to cross. This fact implies that fractional instantons residing on the set of BPS color lines and the set of anti-BPS color lines are noninteracting; namely, they do not exert any static force. In such circumstances, we have already observed that our moduli matrix formalism allows non-BPS exact solutions of field equations [79]. The moduli matrix of the exact solution can be given by

$$H_0 = \begin{pmatrix} 1, & \lambda_1 e^{i\theta_1} e^{\frac{2\pi}{N_{\rm F}} z}, & 0, & 0, & \dots \\ 0, & 0, & 1, & \lambda_2 e^{i\theta_2} e^{-\frac{2\pi}{N_{\rm F}} \bar{z}}, & \dots \end{pmatrix}. \tag{5.14}$$

To visualize the brane picture more exactly, we compute Σ, defined in Eq. (3.3), for this charged bion. Since Σ turned out to be diagonal (reflecting the fact that two fractional instantons on different color lines are noninteracting), we can exactly compute Σ from the moduli matrix (5.14). The plot of Σ in Fig. 27 with the parameter set $\lambda_1 = 10^2$, $\lambda_2 = 10^2$, $N_{\rm F} = 4$ nicely realizes the brane picture that is schematically drawn in Fig. 26(a).

For larger Grassmann sigma models, there are more combinations. An example of a charged bion in $Gr_{6,3}$ is shown in Fig. 26(b).

6. Interaction of Grassmann bions

6.1. Neutral bions

In this section, we calculate the (normalized) energy density $s(x^1)$ and topological-charge density $q(x^1)$ defined as

$$s\left(x^1\right) = \int dx^2 \frac{1}{2\pi v^2} \mathcal{L}\left(x^1, x^2\right), \quad Q = \int dx^1 q\left(x^1\right), \tag{6.1}$$

for the Grassmann-model-specific neutral bion configurations with (1, 1) in Eq. (5.5) and in Fig. 21(c) in Sect. 5.1. We take the separation between the instanton (at $(N_{\rm F}/2\pi)\log\lambda_1$) and anti-instanton (at $-(N_{\rm F}/2\pi)\log\lambda_2$) as a single parameter $\tau = -(N_{\rm F}/2\pi)\log\lambda_1\lambda_2$. From now on, we refer to the

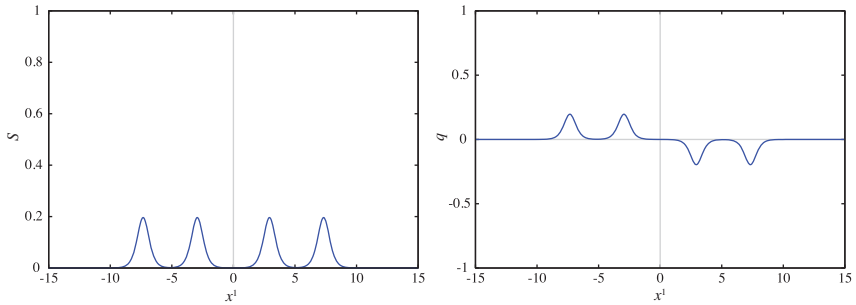

Fig. 28. Energy density $s(x^1)$ (left) and topological charge density $q(x^1)$ (right) for the neutral bion (1, 1) in Eq. (5.5) and in Fig. 21(c) for $\lambda_1 = 10^{-2},\ \lambda_2 = 10^{-2},\ \lambda_3 = 10^{-5},\ \lambda_4 = 10^{-5},\ N_{\rm F} = 4$.

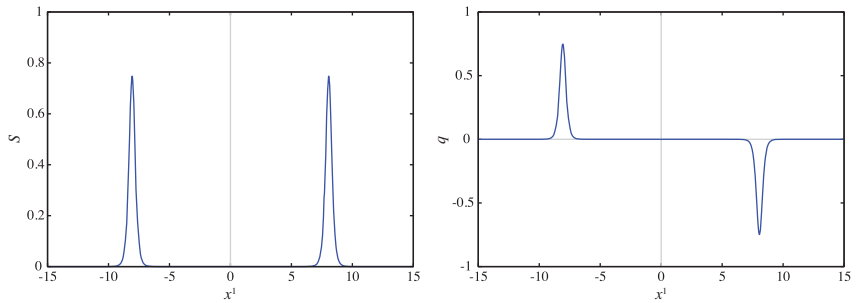

Fig. 29. Energy density $s(x^1)$ (left) and topological charge density $q(x^1)$ (right) for the configuration of Eq. (5.5) for $\lambda_1 = 10^{-6},\ \lambda_2 = 10^{-6},\ \lambda_3 = 10^{-5},\ \lambda_4 = 10^{-5},\ N_{\rm F} = 4$.

instanton at $\pm(N_{\rm F}/2\pi)\log\lambda_i$ just as λ_i. In most of the numerical study, we fix λ_3 and λ_4 as $\lambda_3 = \lambda_4 = 10^5$, then vary λ_1 and λ_2 with the symmetric condition $\lambda_1 = \lambda_2 = \lambda$, unless stated otherwise.

Before discussing the results of the numerical evaluation, we make some comments: First, we take the phase parameter $\theta_i = 0$ $(i = 1, 2, 3, 4)$ for simplicity. Indeed, we find that nonzero θ_i just increases the total energy as with the neutral bion in the $\mathbb{C}P^{N-1}$ model [17], thus $\theta_i = 0$ is a natural choice of phase parameters. Second, we do not show the x^2 axis in the energy and charge density figures, since the energy and charge densities of the BPS fractional instanton, neutral bions, and charged bions are independent of x^2, unlike in the case of the BPS instanton, as shown in Sect. 3.4.

To figure out the properties of this configuration, we depict the energy and charge densities for three sets of parameters:

$$\lambda_1 = 10^{-2},\ \lambda_2 = 10^{-2},\ \lambda_3 = 10^{-5},\ \lambda_4 = 10^{-5},\ N_{\rm F} = 4 \tag{6.2}$$

in Fig. 28;

$$\lambda_1 = 10^{-6},\ \lambda_2 = 10^{-6},\ \lambda_3 = 10^{-5},\ \lambda_4 = 10^{-5},\ N_{\rm F} = 4 \tag{6.3}$$

in Fig. 29; and

$$\lambda_1 = 1,\ \lambda_2 = 1,\ \lambda_3 = 10^{-5},\ \lambda_4 = 10^{-5},\ N_{\rm F} = 4 \tag{6.4}$$

in Fig. 30, respectively.

For $1 \ll \lambda < 10^5$, this configuration is composed of four kinks, two BPS fractional instantons $(S = 1/4,\ Q = 1/4)$ and two BPS fractional anti-instantons $(S = 1/4,\ Q = -1/4)$, which are separately located as shown in Fig. 28. For $\lambda \gtrsim 10^5$, the two instantons are merged into one compressed fractional instanton $(S = 1/2,\ Q = 1/2)$ while the two anti-instantons are merged into one compressed fractional anti-instanton $(S = 1/2,\ Q = -1/2)$, as shown in Fig. 29. It is notable that the

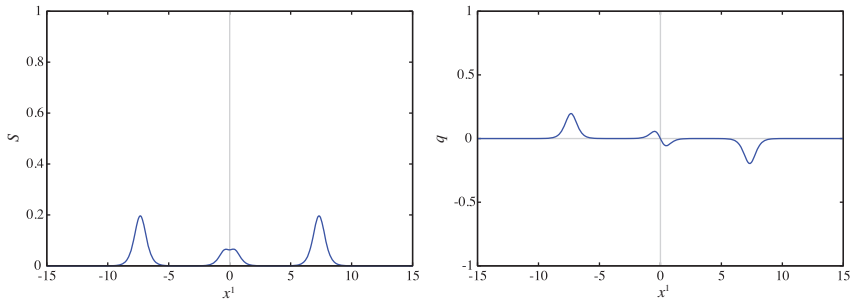

Fig. 30. Energy density $s(x^1)$ (left) and topological charge density $q(x^1)$ (right) for the configuration of Eq. (5.5) for $\lambda_1 = 1, \lambda_2 = 1, \lambda_3 = 10^{-5}, \lambda_4 = 10^{-5}, N_F = 4$.

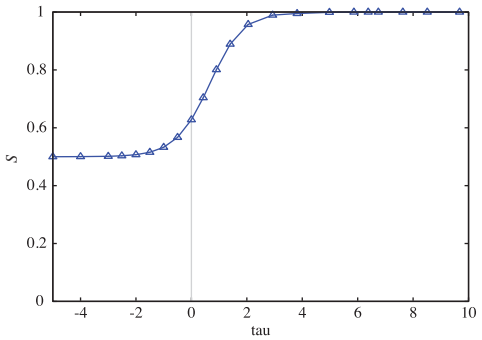

Fig. 31. The total energy as a function of $\tau = -(N_F/\pi)\log\lambda$ with $\lambda = \lambda_1 = \lambda_2$ for $\lambda_3 = \lambda_4 = 10^{-5}$ with $N_F = 4$ fixed.

size of the fractional (anti-)instantons becomes half as large ($\sim 4 \to \sim 2$) when they are compressed with another (anti-)instanton, which is consistent with the argument in Sect. 2.3 (size of instanton $= 1/\Delta m = L/S$). In this case, the total energy is unchanged. For $\lambda \lesssim 1$, the instanton and the anti-instanton characterized by λ_1 and λ_2 respectively are annihilated and disappear, producing one instanton ($S = 1/4$, $Q = 1/4$) and one anti-instanton ($S = 1/4$, $Q = -1/4$), as shown in Fig. 30. In this case, the total energy reduces from $S = 1/4 \times 4 = 1$ to $S = 1/4 \times 2 = 1/2$.

Next, we calculate the parameter dependence of the total energy for the neutral bion configuration (5.5). As a characteristic case, we again vary $\lambda = \lambda_1 = \lambda_2$ with $\lambda_3 = \lambda_4 = 10^{-5}$ fixed. The result is given in Fig. 31. $\tau \sim 10$ corresponds to the compressed-kink cases of Fig. 29, while $\tau = 1$ corresponds to the pair-annihilation case between the instanton and anti-instanton of Fig. 30. The total energy is changed from $S = 4 \times 1/4 = 1$ to $S = 2 \times 1/4 = 1/2$ as τ gets smaller. Since it is known that BPS solitons do not exert any static force, this result shows that there is an attractive static force between the fractional instanton λ_1 and the anti-instanton λ_2.

In order to study mutual interactions between constituent fractional (anti-)instantons more quantitatively, we define the interaction energy density as the energy density $s(x^1)$ minus the two fractional-instanton density and two fractional-anti-instanton density $2s_{\nu=1/N_F} + 2s_{\nu=-1/N_F}$,

$$s_{\rm int}(x^1) = s(x^1) - \left(2s_{\nu=1/N_F} + 2s_{\nu=-1/N_F}\right). \tag{6.5}$$

The integrated interaction energy is then given by

$$S_{\rm int}(N_F, \lambda_1, \lambda_2, \lambda_3, \lambda_4) = \int dx^1\, s_{\rm int}(x^1). \tag{6.6}$$

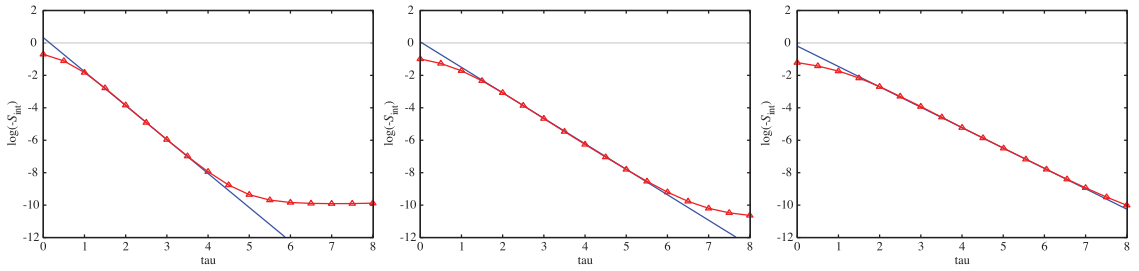

Fig. 32. Plot of $\log(-S_{\rm int}(N_{\rm F},\tau))$ as a function of τ for $N_{\rm F}=3$ (left), $N_{\rm F}=4$ (center), and $N_{\rm F}=5$ (right) for (5.5) (red curves with triangle points). For the intermediate region of τ, the curve is approximated by $-(2\pi/N_{\rm F})\tau + C\big(N_{\rm F}\big)$ (blue curves).

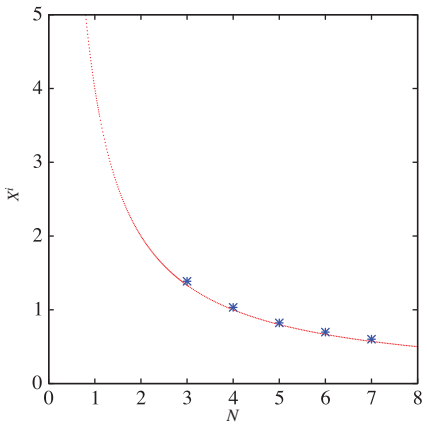

Fig. 33. The constant $\exp\big[C\big(N_{\rm F}\big)\big]$ as a function of $N_{\rm F}$ for $N_{\rm F}=3,4,5,6,7$ (blue points). It is well approximated by $4/N_{\rm F}$ (red curve).

Let us first study the interaction between λ_1 and λ_2. By varying τ with $\lambda_3=\lambda_4=10^{-5}$ fixed, we show the logarithm of the total interaction energy $S_{\rm int}(N_{\rm F},\tau)$ as a function of τ for $N_{\rm F}=3,4,5$ in Fig. 32. For the intermediate separation of τ, $\log(-S_{\rm int}(N_{\rm F},\tau))$ is well approximated by the analytic function

$$\log\big[-S_{\rm int}\big(N_{\rm F},\tau\big)\big] \sim -\frac{2\pi}{N_{\rm F}}\tau + C\big(N_{\rm F}\big), \tag{6.7}$$

where $C(N_{\rm F})$ is a y-intercept. In Fig. 32 we simultaneously depict these analytic functions. The slope $2\pi/N_{\rm F}$ of this line is equivalent to that of the elementary neutral bion in the $\mathbb{C}P^{N_{\rm F}-1}$ model [17], which contains only one fractional instanton and one fractional anti-instanton. This means that the interaction energy is dominated by the interaction between λ_1 and λ_2, and not by the other interactions. In Fig. 33 we plot $\exp[C(N_{\rm F})]$ as a function of $N_{\rm F}$ for $N_{\rm F}=3,4,5,6,7$. By fitting the $N_{\rm F}$ dependence of the constant $C(N_{\rm F})$, we obtain an interaction energy formula identical to the $\mathbb{C}P^{N_{\rm F}-1}$ model [17], which means $C_{N_{\rm F}}\sim 4/N_{\rm F}$. (We note that we have included the factor $1/(2\pi)$ in the definition of the Lagrangian in Eq. (2.19) in this paper compared to our previous paper [17].) Namely, we find

$$S_{\rm int}\big(N_{\rm F},\tau\big) \sim -\frac{4}{N_{\rm F}}\, e^{-\big(2\pi/N_{\rm F}\big)\tau}, \tag{6.8}$$

in the intermediate region where none of the constituent instantons are too close.

Next we study the interaction between the fractional instanton λ_3 and the anti-instanton λ_4 in the outer pair. To isolate the interaction between the outer pair, we take the annihilation limit of the inner pair, fixing the parameters $\lambda_1 = \lambda_2 = 10^5$. Then practically no remnant is left from the inner pair. By varying the separation between λ_3 and λ_4, we find that the interaction energy is given precisely by the same formula as in the case of the inner pair λ_1 and λ_2 in Eq. (6.8). By using this formula for the outer pair, we can see that the contribution from the outer pair becomes tiny in the geometrical configurations in Figs. 28, 29, and 30. This justifies the neglect of the outer pair interaction energy in analyzing the interaction energy of the inner pair a posteriori.

With our level of numerical accuracy, we cannot obtain definite results for the other possible interactions between the fractional instanton and the anti-fractional instanton residing on different color lines, such as $\lambda_1 - \lambda_4$ and $\lambda_3 - \lambda_2$, except that they are at least as small as the interaction energy between the outer pair at the same separation.

At the end of this subsection, we comment on the hierarchy of the fractional instanton size, the neutral bion size, and the instanton separation.

1. The fractional instanton size is given by $\tau \sim 1$. (The compact scale L is omitted.)
2. The neutral bion size is determined by the separation scale at which the interaction energy coincides with the approximate form (6.8), which is larger than $\tau \sim 1$. This form is consistent with Dunne–Ünsal's result, and works to cancel the renormalon ambiguity in the perturbative calculation [8,9].
3. The typical fractional-instanton separation is determined by the scale where the fractional instantons behave as if they have no interaction. This scale is much larger than the bion size, and is parametrically given by $\tau \sim e^{1/g^2}$ [8,9].

Although we have not considered running coupling and dimensional transmutation in our analysis, the hierarchy we found is qualitatively consistent with $1 \ll \log\left(1/g^2\right) \ll e^{1/g^2}$, which is shown by Ünsal and his collaborators.

6.2. *Charged bions*

We next consider the charged bion in the Grassmann sigma model. For the $Gr_{4,2}$ model, we found only one irreducible charged bion with the fractional instanton number $(-1, 1)$ in Fig. 26(a), which is given by the moduli matrix in Eq. (5.14). This is an exact non-BPS solution, since the BPS and anti-BPS sectors reside on color branes that do not share any common flavors, and are noninteracting.

To find out the properties of the solution in detail, we study it numerically using our formula in Eq. 2.24. We observe analytically that the energy and charge densities are independent of the moduli parameters θ_1 and θ_2. For the symmetric case $\lambda \equiv \lambda_1 = \lambda_2$, the separation between the fractional instanton (at $-(N_{\rm F}/2\pi)\log\lambda_1$) and fractional anti-instanton (at $(N_{\rm F}/2\pi)\log\lambda_2$) is given by $\tau = (N_{\rm F}/\pi)\log\lambda$. We depict energy and charge densities for three sets of parameters:

$$\lambda_1 = 10^2, \quad \lambda_2 = 10^2, \quad N_{\rm F} = 4, \tag{6.9}$$

$$\lambda_1 = 10, \quad \lambda_2 = 10, \quad N_{\rm F} = 4, \tag{6.10}$$

$$\lambda_1 = 1, \quad \lambda_2 = 1, \quad N_{\rm F} = 4. \tag{6.11}$$

Figures 34, 35, and 36 show the results.

We find that, unlike the neutral bions, the energy density is still nonzero even in the no separation limit $\tau = 0$ ($\lambda_1 = \lambda_2 = 1$) of the fractional instanton and anti-instanton. As shown in Fig. 36, lumps of the topological charge density annihilate and disappear in this case. Although the total topological

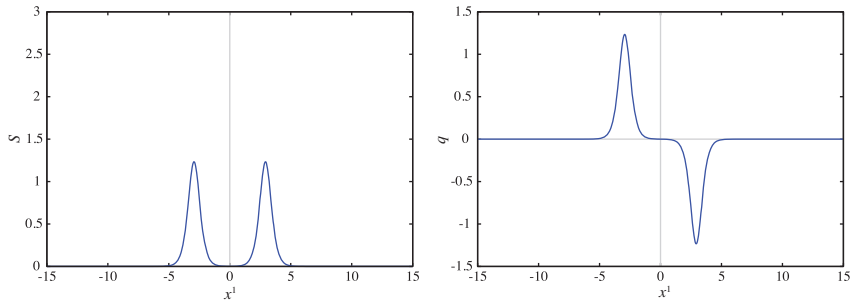

Fig. 34. Energy density $s(x^1)$ (left) and topological charge density $q(x^1)$ (right) for the configuration of Eq. (5.14) for $\lambda_1 = 10^2,\ \lambda_2 = 10^2,\ N_F = 4$.

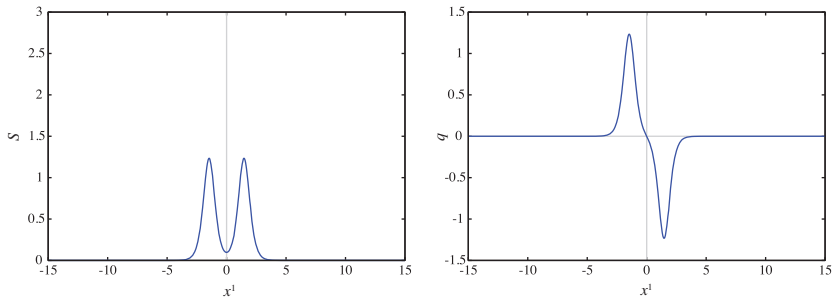

Fig. 35. Energy density $s(x^1)$ (left) and topological charge density $q(x^1)$ (right) for the configuration of Eq. (5.14) for $\lambda_1 = 10,\ \lambda_2 = 10,\ N_F = 4$.

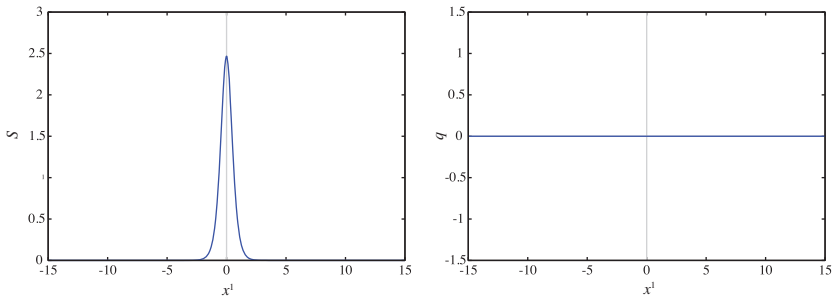

Fig. 36. Energy density $s(x^1)$ (left) and topological charge density $q(x^1)$ (right) for the configuration of Eq. (5.14) for $\lambda_1 = 1,\ \lambda_2 = 1,\ N_F = 4$.

charge happens to vanish, the BPS fractional instanton and anti-instanton are not of the same species, and cannot annihilate each other, as anticipated. To show details, we depict the separation (τ) dependence of the total energy in Fig. 37. The total energy is independent of the separation, and keeps a constant value $S = 2 \times 1/4 = 1/2$. This result supports the notion that the positions as well as the phases of (anti-)fractional instantons are moduli of the exact solution of the charged bion in the Grassmann sigma model, even though it is non-BPS. This is consistent with the argument that the instability and ambiguity in the neutral bion amplitude encode the IR renormalon in the perturbative expansion series, while the charged bions are not directly relevant. Rather, it should contribute to the dynamics such as confinement of the theory.

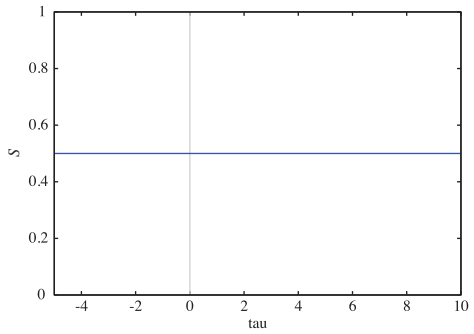

Fig. 37. The total energy of the charged bions as a function of $\tau = (N_{\rm F}/\pi)\log\lambda$ with $\lambda = \lambda_1 = \lambda_2$ for $N_{\rm F} = 4$ fixed.

7. Summary and discussion

In this paper, we have considered topologically trivial configurations in the Grassmann sigma model on $\mathbb{R}^1 \times S^1$ with the $\mathbb{Z}_{N_{\rm F}}$ symmetric twisted boundary conditions, to study the properties of bions composed of multiple fractional instantons. By formulating these models as gauge theories, we proposed to use the moduli matrix to classify bion configurations. By embedding these models into D-brane configurations in type-II string theories, we have found that D-brane configurations, together with the moduli matrix, are useful to classify all possible bion configurations in the $\mathbb{C}P^{N_{\rm F}-1}$ models and the Grassmann sigma models. We have found that the Grassmann sigma models admit neutral bions made of BPS and anti-BPS fractional instantons, each of which has a topological charge greater (less) than one (minus one); nevertheless, they cannot be decomposed into (anti-)instantons and the rest. We have found that Grassmann models admit charged bions, while the $\mathbb{C}P^{N_{\rm F}-1}$ models do not admit them. We have also constructed exact solutions of charged bions in the Grassmann model. We have calculated the energy density and topological charge density of the bion configurations in these models numerically, and have obtained their interactions. The dependence of these interactions on the separations between fractional instanton constituents is studied explicitly.

We have studied the Grassmann sigma model without fermions. On the other hand, fermions can be coupled to the Grassmann sigma model. This is the case of the supersymmetric Grassmann sigma model, which can be formulated from supersymmetric gauge theories. In this case, fermions are localized at the fractional instantons and contribute to the interactions between bions.

In this paper, we have concentrated on the $\mathbb{Z}_{N_{\rm F}}$ symmetric twisted boundary conditions, where the z dependence of the moduli matrix appears in powers of $e^{2\pi z/N_{\rm F}}$. Consequently, the topological charge of fractional instantons is proportional to $1/N_{\rm F}$, and the flavor branes are equally spaced in D-brane configurations. Consideration of more general boundary conditions remains as a future problem. The classification of fractional instantons and bions by the moduli matrix and D-brane configurations is essentially the same as long as the boundary conditions of different flavor components are not degenerated. More precisely, when the boundary condition of the scalar fields of the flavor component f is $H_f(x^1, x^2+1) = H_f(x^1, x^2)e^{i\alpha_f}$, the elementary fractional instantons have the instanton charges $\alpha_{f+1} - \alpha_f$. Consequently, the z dependence of the moduli matrix of the flavor component f appears in the form of $e^{\alpha_f z}$, and flavor branes are not equidistant in D-brane configurations. On the other hand, unbroken gauge symmetry occurs for gauge theory on $\mathbb{R}^3 \times S^1$ with partially degenerated twisted boundary conditions. We can prepare corresponding situations by putting boundary conditions of some flavors to coincide. In this case, kinks carry non-Abelian

moduli and can be called non-Abelian kinks [97–99]. In the brane picture, the s-rule admits at most n color branes to sit on n coincident flavor branes, and there remains a $U(n)$ gauge symmetry on the color branes, which is a source of non-Abelian moduli for non-Abelian kinks. We will consider this situation with "non-Abelian bions" in a future publication.

One of the future directions is to extend our method to bion configurations in other nonlinear sigma models. Since nonlinear sigma models on Hermitian symmetric space (including Grassmann and $\mathbb{C}P^{N_{\rm F}-1}$) can be formulated as gauge theories [53], the moduli matrix can be used for these cases, although embedding into brane configurations is not yet available. From the gauge theory perspective, changing the gauge group from $U\left(N_{\rm C}\right)$, studied in this paper, to other groups is also one possible direction. The (hyper-)Kähler quotients for $G = SO$ and USp were obtained in Ref. [100], in which fractional instantons were also studied. We may study bions in these cases.

As for the relation between 2- and 4D theories, the effective theory on a non-Abelian vortex in four dimensions [58,59,62–64] is the 2D $\mathbb{C}P^{N_{\rm F}-1}$ model; therefore, the Yang–Mills instantons and monopoles are $\mathbb{C}P^{N_{\rm F}-1}$ instantons and kinks inside a vortex, respectively [60,66,66,67,101,102]. Therefore, bions in Yang–Mills theory can exist inside the vortex as the $\mathbb{C}P^{N_{\rm F}-1}$ bions when the vortex worldsheet is wrapped around S^1. In this regard, a non-Abelian vortex in gauge theories with gauge group G admits a G/H nonlinear sigma model on its worldsheet [103]. In particular, the cases of $G = SO(N)$ and $USp(2N)$ have been studied extensively [100,104,105]. With twisted boundary conditions, they admit monopoles as kinks on G/H sigma models in the vortex theory [106], in which a kinky brane-like picture was obtained. Quark matter in high-density QCD also admits a non-Abelian vortex [107,108] whose effective theory is the $\mathbb{C}P^2$ model [109,110] (see Ref. [111] for a review). A bound state of a kink and an anti-kink appears quantum mechanically inside a vortex, representing a meson of a monopole and an anti-monopole. The quark–hadron duality between the confining phase at low density and the Higgs phase at high density may be explained through a non-Abelian vortex [112]. Bions inside a non-Abelian vortex wrapped around S^1 in these cases will be interesting to study in the future.

We may compactify two or more directions in higher-dimensional theories. For instance, the $\mathbb{C}P^{N_{\rm F}-1}$ model, Grassmann sigma model, and corresponding gauge theories on $\mathbb{R}^2 \times S^1 \times S^1$ admit not only fractional lumps (vortices) from one of the S^1, which are string-like, linearly extended structures of the fractional instantons studied in this paper, but also their intersections with the Yang–Mills instanton charge [102]. These configurations are called amoebas in mathematics and reduce to domain wall junctions [113–116] for a small S^1 radii limit. Bions in this theory will have more varieties because fractional solitons have networks in two directions, and hopefully will be useful for 4D gauge theories.

Acknowledgements

We are grateful to Mithat Ünsal and Gerald Dunne for their interest and valuable comments and correspondence on their related work during the entire course of our study. T.M. and N.S. thank Philip Argyres, Alexei Cherman, Falk Bruckmann, Tin Sulejmanpasic, and other participants of CERN Theory Institute 2014, "Resurgence and Transseries in Quantum, Gauge and String theories" for the fruitful discussion and useful correspondence. T.M. is in part supported by the Japan Society for the Promotion of Science (JSPS) Grants Number 26800147. The work of M.N. is supported in part by a Grant-in-Aid for Scientific Research (No. 25400268) and by the "Topological Quantum Phenomena" Grant-in-Aid for Scientific Research on Innovative Areas (No. 25103720) from the Ministry of Education, Culture, Sports, Science and Technology (MEXT) of Japan. N.S. is supported by a Grant-in Aid for Scientific Research No. 25400241 from the Ministry of Education, Culture, Sports, Science and Technology (MEXT) of Japan.

Funding

Open Access funding: SCOAP[3].

Appendix A. The solution of the constraint $HH^\dagger = v^2 \mathbf{1}_{N_C}$

Since the gauge-invariant quantity Ω is a nonnegative Hermitian $N_C \times N_C$ matrix, we can diagonalize it by a unitary matrix U to obtain a nonnegative diagonal matrix Ω_d, as given in Eq. (2.23). Since Ω depends on both z and $\bar{z}$, matrices U and Ω_d also depend on z and $\bar{z}$. Any (non-integer) α powers of a Hermitian matrix can be defined as

$$\Omega^\alpha = U \Omega_d^\alpha U^\dagger. \tag{A1}$$

One can choose $\alpha = -1/2$ to define the inverse square root $\Omega^{-1/2}$ as a solution for S^{-1}. Thus we find a possible representative of the physical scalar field H as in Eq. (2.24). It is easy to see that the solution satisfies the remaining constraint (2.2):

$$\begin{aligned} HH^\dagger &= U\Omega_d^{-1/2}U^{-1}H_0H_0^\dagger U\Omega_d^{-1/2}U^{-1} = v^2 U\Omega_d^{-1/2}U^{-1}\Omega U\Omega_d^{-1/2}U^{-1} \\ &= v^2 U\Omega_d^{-1/2}U^{-1}H_0 U\Omega_d U^\dagger U\Omega_d^{-1/2}U^{-1} = v^2 \mathbf{1}_{N_C}. \end{aligned} \tag{A2}$$

The V-transformations defined in Eq. (2.12) give different representatives for the moduli matrix $H_0' = VH_0$, $V \in GL(N_C, \mathbb{C})$. The V-transformed H_0' gives a covariant Ω' in Eq. (2.13):

$$v^2\Omega' = H_0' H_0'^\dagger = VH_0H_0'V^\dagger = v^2 V\Omega V^\dagger = v^2 VU\Omega_d U^\dagger V^\dagger. \tag{A3}$$

We can diagonalize Ω' with a unitary matrix U' to give a diagonal matrix Ω_d':

$$\Omega' = U'\Omega_d' U'^\dagger. \tag{A4}$$

Therefore, we can obtain another scalar field H':

$$H' = U'\Omega_d'^{-1/2}U'^\dagger H_0', \tag{A5}$$

which satisfies the constraint

$$H'H'^\dagger = v^2 \mathbf{1}_{N_C}. \tag{A6}$$

However, VU is not unitary, and is different from U'. Even the eigenvalues are different: $\Omega_d' \neq \Omega_d$. Therefore, the resulting solution H' of the constraint obtained from Eq. (2.24) is in general different from H. Although relations between U', Ω_d' and U, Ω are complicated, we find that the following matrix $\tilde{U}$

$$\tilde{U} = \frac{1}{v^2} H'H^\dagger \tag{A7}$$

is a unitary matrix

$$\begin{aligned} \tilde{U}\tilde{U}^\dagger &= \frac{1}{v^4}\left(U'\Omega_d'^{-1/2}U'^\dagger VH_0H_0^\dagger U\Omega_d^{-1/2}U^\dagger\right)\left(U\Omega_d^{-1/2}U^\dagger H_0H_0^\dagger V^\dagger U'\Omega_d'^{-1/2}U'^\dagger\right) \\ &= U'\Omega_d'^{-1/2}U'^\dagger V\Omega V^\dagger U'\Omega_d'^{-1/2}U'^\dagger \mathbf{1}_{N_C}. \end{aligned} \tag{A8}$$

This relation, together with the relations in Eqs. (A2) and (A6), implies

$$H' = \tilde{U}H. \tag{A9}$$

Namely, H' and H are $U(N_C)$ gauge transformations of each other.

References

[1] M. Ünsal, Phys. Rev. Lett. **100**, 032005 (2008) [arXiv:0708.1772 [hep-th]] [Search INSPIRE].
[2] M. Ünsal, Phys. Rev. D **80**, 065001 (2009) [arXiv:0709.3269 [hep-th]] [Search INSPIRE].
[3] M. Shifman and M. Ünsal, Phys. Rev. D **78**, 065004 (2008) [arXiv:0802.1232 [hep-th]] [Search INSPIRE].
[4] E. Poppitz and M. Ünsal, J. High Energy Phys. **0909**, 050 (2009) [arXiv:0906.5156 [hep-th]] [Search INSPIRE].
[5] E. Poppitz, T. Schaefer, and M. Ünsal, J. High Energy Phys. **1210**, 115 (2012) [arXiv:1205.0290 [hep-th]] [Search INSPIRE].
[6] P. Argyres and M. Ünsal, Phys. Rev. Lett. **109**, 121601 (2012) [arXiv:1204.1661 [hep-th]] [Search INSPIRE].
[7] P. C. Argyres and M. Ünsal, J. High Energy Phys. **1208**, 63 (2012) [arXiv:1206.1890 [hep-th]] [Search INSPIRE].
[8] G. V. Dunne and M. Ünsal, J. High Energy Phys. **1211**, 170 (2012) [arXiv:1210.2423 [hep-th]] [Search INSPIRE].
[9] G. V. Dunne and M. Ünsal, Phys. Rev. D **87**, 025015 (2013) [arXiv:1210.3646 [hep-th]] [Search INSPIRE].
[10] R. Dabrowski and G. V. Dunne, Phys. Rev. D **88**, 025020 (2013) [arXiv:1306.0921 [hep-th]] [Search INSPIRE].
[11] G. V. Dunne and M. Ünsal, Phys. Rev. D **89**, 041701 (2014) [arXiv:1306.4405 [hep-th]] [Search INSPIRE].
[12] A. Cherman, D. Dorigoni, G. V. Dunne, and M. Ünsal, Phys. Rev. Lett. **112**, 021601 (2014) [arXiv:1308.0127 [hep-th]] [Search INSPIRE].
[13] G. Basar, G. V. Dunne, and M. Ünsal, J. High Energy Phys. **1310**, 041 (2013) [arXiv:1308.1108 [hep-th]] [Search INSPIRE].
[14] G. V. Dunne and M. Ünsal, Phys. Rev. D **89**, 105009 (2014) [arXiv:1401.5202 [hep-th]] [Search INSPIRE].
[15] A. Cherman, D. Dorigoni, and M. Ünsal, [arXiv:1403.1277 [hep-th]] [Search INSPIRE].
[16] S. Bolognesi and W. Zakrzewski, Phys. Rev. D **89**, 065013 (2014) [arXiv:1310.8247 [hep-th]] [Search INSPIRE].
[17] T. Misumi, M. Nitta, and N. Sakai, J. High Energy Phys. **1406**, 164 (2014) [arXiv:1404.7225 [hep-th]] [Search INSPIRE].
[18] T. Misumi and T. Kanazawa, J. High Energy Phys. **1406**, 181 (2014) [arXiv:1405.3113 [hep-ph]] [Search INSPIRE].
[19] Y. Hosotani, Phys. Lett. B **126**, 309 (1983).
[20] Y. Hosotani, Annals Phys. **190**, 233 (1989).
[21] J. C. Myers and M. C. Ogilvie, Phys. Rev. D **77**, 125030 (2008) [arXiv:0707.1869 [hep-lat]] [Search INSPIRE].
[22] J. C. Myers and M. C. Ogilvie, J. High Energy Phys. **0907**, 095 (2009) [arXiv:0903.4638 [hep-th]] [Search INSPIRE].
[23] G. Cossu and M. D'Elia, J. High Energy Phys. **0907**, 048 (2009) [arXiv:0904.1353 [hep-lat]] [Search INSPIRE].
[24] P. N. Meisinger and M. C. Ogilvie, Phys. Rev. D **81**, 025012 (2010) [arXiv:0905.3577 [hep-lat]] [Search INSPIRE].
[25] H. Nishimura and M. C. Ogilvie, Phys. Rev. D **81**, 014018 (2010) [arXiv:0911.2696 [hep-lat]] [Search INSPIRE].
[26] M. M. Anber and E. Poppitz, J. High Energy Phys. **1106**, 136 (2011) [arXiv:1105.0940 [hep-th]] [Search INSPIRE].
[27] M. C. Ogilvie, J. Phys. A **45**, 483001 (2012) [arXiv:1211.2843 [hep-th]] [Search INSPIRE].
[28] K. Kashiwa and T. Misumi, J. High Energy Phys. **1305**, 042 (2013) [arXiv:1302.2196 [hep-ph]] [Search INSPIRE].
[29] G. Cossu, H. Hatanaka, Y. Hosotani, and J. I. Noaki, Phys. Rev. D **89**, 094509 (2014) [arXiv:1309.4198 [hep-lat]] [Search INSPIRE].
[30] G. 't Hooft, Subnucl. Ser. **15**, 943 (1979).

[31] V. A. Fateev, V. A. Kazakov, and P. B. Wiegmann, Nucl. Phys. B **424**, 505 (1994) [arXiv:9403099 [hep-th]] [Search INSPIRE].
[32] V. A. Fateev, P. B. Wiegmann, and V. A. Kazakov, Phys. Rev. Lett. **73**, 1750 (1994).
[33] J. Ecalle, *Les Fonctions Resurgentes* (Publ. Math. Orsay, Universite de Paris-Sud, Departement de Mathematique, 1981), Vols. I–III.
[34] E. B. Bogomolny, Phys. Lett. B **91**, 431 (1980).
[35] J. Zinn-Justin, Nucl. Phys. B **192**, 125 (1981).
[36] J. Zinn-Justin and U. D. Jentschura, Annals Phys. **313**, 197 (2004) [arXiv:0501136 [quant-ph]] [Search INSPIRE].
[37] A. M. Polyakov, *Gauge Fields and Strings: Contemporary Concepts in Physics* (Harwood, London, 1989).
[38] A. M. Polyakov and A. A. Belavin, JETP Lett. **22**, 245 (1975) [Pisma Zh. Eksp. Teor. Fiz. **22**, 503 (1975)].
[39] A. M. Din and W. J. Zakrzewski, Nucl. Phys. B **174**, 397 (1980).
[40] A. M. Din and W. J. Zakrzewski, Nucl. Phys. B **182**, 151 (1981).
[41] W. J. Zakrzewski, *Low Dimensional Sigma Models* (IOP Publ. Bristol, UK, 1989).
[42] M. Eto, Y. Isozumi, M. Nitta, K. Ohashi, and N. Sakai, Phys. Rev. D **72**, 025011 (2005) [arXiv:0412048 [hep-th]] [Search INSPIRE].
[43] F. Bruckmann, Phys. Rev. Lett. **100**, 051602 (2008) [arXiv:0707.0775 [hep-th]] [Search INSPIRE].
[44] W. Brendel, F. Bruckmann, L. Janssen, A. Wipf, and C. Wozar, Phys. Lett. B **676**, 116 (2009) [arXiv:0902.2328 [hep-th]] [Search INSPIRE].
[45] D. Harland, J. Math. Phys. **50**, 122902 (2009) [arXiv:0902.2303 [hep-th]] [Search INSPIRE].
[46] F. Bruckmann and T. Sulejmanpasic, [arXiv:1408.2229 [hep-th]] [Search INSPIRE].
[47] M. Eto, T. Fujimori, Y. Isozumi, M. Nitta, K. Ohashi, K. Ohta, and N. Sakai, Phys. Rev. D **73**, 085008 (2006) [arXiv:0601181 [hep-th]] [Search INSPIRE].
[48] M. Eto, T. Fujimori, M. Nitta, K. Ohashi, K. Ohta, and N. Sakai,Nucl. Phys. B **788**, 120 (2008) [arXiv:0703197 [hep-th]] [Search INSPIRE].
[49] E. B. Bogomolny, Sov. J. Nucl. Phys. **24**, 449 (1976) [Yad. Fiz. **24**, 861 (1976)].
[50] M. K. Prasad and C. M. Sommerfield, Phys. Rev. Lett. **35**, 760 (1975).
[51] A. D'Adda, P. Di Vecchia, and M. Luscher, Nucl. Phys. B **152**, 125 (1979).
[52] S. Aoyama, Nuovo Cimento A **57**, 176 (1980).
[53] K. Higashijima and M. Nitta, Prog. Theor. Phys. **103**, 635 (2000) [arXiv:9911139 [hep-th]] [Search INSPIRE].
[54] U. Lindström and M. Roček, Nucl. Phys. B **222**, 285 (1983).
[55] N. J. Hitchin, A. Karlhede, U. Lindström, and M. Roček, Commun. Math. Phys. **108**, 535 (1987).
[56] I. Antoniadis and B. Pioline, Int. J. Mod. Phys. A **12**, 4907 (1997) [arXiv:9607058 [hep-th]] [Search INSPIRE].
[57] M. Arai, M. Nitta, and N. Sakai, Prog. Theor. Phys. **113**, 657 (2005) [arXiv:0307274 [hep-th]] [Search INSPIRE].
[58] A. Hanany and D. Tong, J. High Energy Phys. **0307**, 037 (2003) [arXiv:0306150 [hep-th]] [Search INSPIRE].
[59] R. Auzzi, S. Bolognesi, J. Evslin, K. Konishi, and A. Yung, Nucl. Phys. B **673**, 187 (2003) [arXiv:0307287 [hep-th]] [Search INSPIRE].
[60] M. Shifman and A. Yung, Phys. Rev. D **70**, 045004 (2004) [arXiv:0403149 [hep-th]] [Search INSPIRE].
[61] A. Hanany and D. Tong, J. High Energy Phys. **0404**, 066 (2004) [arXiv:0403158 [hep-th]] [Search INSPIRE].
[62] M. Eto, Y. Isozumi, M. Nitta, K. Ohashi, and N. Sakai, Phys. Rev. Lett. **96**, 161601 (2006) [arXiv:0511088 [hep-th]] [Search INSPIRE].
[63] M. Eto, K. Konishi, G. Marmorini, M. Nitta, K. Ohashi, W. Vinci, and N. Yokoi, Phys. Rev. D **74**, 065021 (2006).
[64] M. Eto, K. Hashimoto, G. Marmorini, M. Nitta, K. Ohashi, and W. Vinci, Phys. Rev. Lett. **98**, 091602 (2007) [arXiv:0609214 [hep-th]] [Search INSPIRE].
[65] D. Tong, [arXiv:0509216 [hep-th]] [Search INSPIRE].
[66] M. Eto, Y. Isozumi, M. Nitta, K. Ohashi, and N. Sakai, J. Phys. A **39**, R315 (2006) [arXiv:0602170 [hep-th]] [Search INSPIRE].

[67] M. Eto, Y. Isozumi, M. Nitta, and K. Ohashi, Nucl. Phys. B **752**, 140 (2006) [arXiv:0506257 [hep-th]] [Search INSPIRE].
[68] M. Shifman and A. Yung, Rev. Mod. Phys. **79**, 1139 (2007) [arXiv:0703267 [hep-th]] [Search INSPIRE].
[69] M. Shifman and A. Yung, *Supersymmetric Solitons* (Cambridge University Press, Cambridge, UK, 2009).
[70] M. Shifman and A. Yung, Phys. Rev. D **73**, 125012 (2006) [arXiv:0603134 [hep-th]] [Search INSPIRE].
[71] M. Eto, J. Evslin, K. Konishi, G. Marmorini, M. Nitta, K. Ohashi, W. Vinci, and N. Yokoi, Phys. Rev. D **76**, 105002 (2007) [arXiv:0704.2218 [hep-th]] [Search INSPIRE].
[72] A. Hanany and E. Witten, Nucl. Phys. B **492**, 152 (1997) [arXiv:9611230 [hep-th]] [Search INSPIRE].
[73] A. Giveon and D. Kutasov, Rev. Mod. Phys. **71**, 983 (1999) [arXiv:9802067 [hep-th]] [Search INSPIRE].
[74] Y. Isozumi, M. Nitta, K. Ohashi, and N. Sakai, Phys. Rev. Lett. **93**, 161601 (2004) [arXiv:0404198 [hep-th]] [Search INSPIRE].
[75] Y. Isozumi, M. Nitta, K. Ohashi, and N. Sakai, Phys. Rev. D **70**, 125014 (2004) [arXiv:0405194 [hep-th]] [Search INSPIRE].
[76] Y. Isozumi, M. Nitta, K. Ohashi, and N. Sakai, Phys. Rev. D **71**, 065018 (2005) [arXiv:0405129 [hep-th]] [Search INSPIRE].
[77] M. Eto, Y. Isozumi, M. Nitta, K. Ohashi, K. Ohta, N. Sakai, and Y. Tachikawa, Phys. Rev. D **71**, 105009 (2005) [arXiv:0503033 [hep-th]] [Search INSPIRE].
[78] N. D. Lambert and D. Tong, Nucl. Phys. B **569**, 606 (2000) [arXiv:9907098 [hep-th]] [Search INSPIRE].
[79] M. Eto, Y. Isozumi, M. Nitta, K. Ohashi, K. Ohta, and N. Sakai, Phys. Rev. D **71**, 125006 (2005) [arXiv:0412024 [hep-th]] [Search INSPIRE].
[80] B. Zumino, Phys. Lett. B **87**, 203 (1979).
[81] L. Alvarez-Gaume and D. Z. Freedman, Commun. Math. Phys. **80**, 443 (1981).
[82] L. Alvarez-Gaume and D. Z. Freedman, Commun. Math. Phys. **91**, 87 (1983).
[83] E. Witten and D. I. Olive, Phys. Lett. B **78**, 97 (1978).
[84] T. Inami, S. Minakami, and M. Nitta, Nucl. Phys. B **752**, 391 (2006) [arXiv:0605064 [hep-th]] [Search INSPIRE].
[85] C. H. Taubes, Commun. Math. Phys. **72**, 277 (1980).
[86] P. C. Argyres, M. R. Plesser, and N. Seiberg, Nucl. Phys. B **471**, 159 (1996) [arXiv:9603042 [hep-th]] [Search INSPIRE].
[87] K. Ohta, N. Sakai, and Y. Yoshida, Prog. Theor. Exp. Phys. **2013**, 073B03 (2013) [arXiv:1303.4961 [hep-th]] [Search INSPIRE].
[88] M. Shifman and A. Yung, Phys. Rev. D **67**, 125007 (2003) [arXiv:0212293 [hep-th]] [Search INSPIRE].
[89] E. R. C. Abraham and P. K. Townsend, Phys. Lett. B **291**, 85 (1992).
[90] E. R. C. Abraham and P. K. Townsend, Phys. Lett. B **295**, 225 (1992).
[91] M. Arai, M. Naganuma, M. Nitta, and N. Sakai, Nucl. Phys. B **652**, 35 (2003) [arXiv:0211103 [hep-th]] [Search INSPIRE].
[92] M. Arai, M. Naganuma, M. Nitta, and N. Sakai, BPS wall in $N = 2$ SUSY nonlinear sigma model with Eguchi–Hanson manifold. In *A Garden of Quanta-In honor of Hiroshi Ezawa*, eds. A. Arai et al. (World Scientific Publishing Co. Pte. Ltd, Singapore, 2003), pp. 299–325 [arXiv:0302028 [hep-th]] [Search INSPIRE].
[93] M. Nitta, Phys. Rev. D **86**, 125004 (2012) [arXiv:1207.6958 [hep-th]] [Search INSPIRE].
[94] M. Kobayashi and M. Nitta, Phys. Rev. D **87**, 085003 (2013) [arXiv:1302.0989 [hep-th]] [Search INSPIRE].
[95] J. P. Gauntlett, D. Tong, and P. K. Townsend, Phys. Rev. D **64**, 025010 (2001) [arXiv:0012178 [hep-th]] [Search INSPIRE].
[96] D. Tong, Phys. Rev. D **66**, 025013 (2002) [arXiv:0202012 [hep-th]] [Search INSPIRE].
[97] M. Shifman and A. Yung, Phys. Rev. D **70**, 025013 (2004) [arXiv:0312257 [hep-th]] [Search INSPIRE].
[98] M. Eto, M. Nitta, K. Ohashi, and D. Tong, Phys. Rev. Lett. **95**, 252003 (2005) [arXiv:0508130 [hep-th]] [Search INSPIRE].

[99] M. Eto, T. Fujimori, M. Nitta, K. Ohashi, and N. Sakai, Phys. Rev. D **77**, 125008 (2008) [arXiv:0802.3135 [hep-th]] [Search INSPIRE].
[100] M. Eto, T. Fujimori, S. B. Gudnason, M. Nitta, and K. Ohashi, Nucl. Phys. B **815**, 495 (2009) [arXiv:0809.2014 [hep-th]] [Search INSPIRE].
[101] D. Tong, Phys. Rev. D **69**, 065003 (2004) [arXiv:0307302 [hep-th]] [Search INSPIRE].
[102] T. Fujimori, M. Nitta, K. Ohta, N. Sakai, and M. Yamazaki, Phys. Rev. D **78**, 105004 (2008) [arXiv:0805.1194 [hep-th]] [Search INSPIRE].
[103] M. Eto, T. Fujimori, S. B. Gudnason, K. Konishi, M. Nitta, K. Ohashi, and W. Vinci, Phys. Lett. B **669**, 98 (2008) [arXiv:0802.1020 [hep-th]] [Search INSPIRE].
[104] M. Eto, T. Fujimori, S. B. Gudnason, K. Konishi, T. Nagashima, M. Nitta, K. Ohashi, and W. Vinci, J. High Energy Phys. **0906**, 004 (2009) [arXiv:0903.4471 [hep-th]] [Search INSPIRE].
[105] L. Ferretti, S. B. Gudnason, and K. Konishi, Nucl. Phys. B **789**, 84 (2008) [arXiv:0706.3854 [hep-th]] [Search INSPIRE].
[106] M. Eto, T. Fujimori, S. B. Gudnason, Y. Jiang, K. Konishi, M. Nitta, and K. Ohashi, J. High Energy Phys. **1112**, 017 (2011) [arXiv:1108.6124 [hep-th]] [Search INSPIRE].
[107] A. P. Balachandran, S. Digal, and T. Matsuura, Phys. Rev. D **73**, 074009 (2006) [arXiv:0509276 [hep-ph]] [Search INSPIRE].
[108] E. Nakano, M. Nitta, and T. Matsuura, Phys. Rev. D **78**, 045002 (2008) [arXiv:0708.4096 [hep-ph]] [Search INSPIRE].
[109] M. Eto, E. Nakano, and M. Nitta, Phys. Rev. D **80**, 125011 (2009) [arXiv:0908.4470 [hep-ph]] [Search INSPIRE].
[110] M. Eto, M. Nitta, and N. Yamamoto, Phys. Rev. Lett. **104**, 161601 (2010) [arXiv:0912.1352 [hep-ph]] [Search INSPIRE].
[111] M. Eto, Y. Hirono, M. Nitta, and S. Yasui, Prog. Theor. Exp. Phys. **2014**, 012D01 (2014) [arXiv:1308.1535 [hep-ph]] [Search INSPIRE].
[112] M. Eto, M. Nitta, and N. Yamamoto, Phys. Rev. D **83**, 085005 (2011) [arXiv:1101.2574 [hep-ph]] [Search INSPIRE].
[113] M. Eto, Y. Isozumi, M. Nitta, K. Ohashi, and N. Sakai, Phys. Rev. D **72**, 085004 (2005) [arXiv:0506135 [hep-th]] [Search INSPIRE].
[114] M. Eto, Y. Isozumi, M. Nitta, K. Ohashi, and N. Sakai, Phys. Lett. B **632**, 384 (2006) [arXiv:0508241 [hep-th]] [Search INSPIRE].
[115] M. Eto, Y. Isozumi, M. Nitta, K. Ohashi, K. Ohta, and N. Sakai, AIP Conf. Proc. **805**, 354 (2006) [arXiv:0509127 [hep-th]] [Search INSPIRE].
[116] M. Eto, T. Fujimori, T. Nagashima, M. Nitta, K. Ohashi, and N. Sakai, Phys. Rev. D **76**, 125025 (2007) [arXiv:0707.3267 [hep-th]] [Search INSPIRE].